nature plants

ARTICLES

https://doi.org/10.1038/s41477-021-01017-6

Non-cell autonomous and spatiotemporal signalling from a tissue organizer orchestrates root vascular development

BaoJun Yang[1,2]✉, Max Minne[1,2], Federica Brunoni[3], Lenka Plačková[3], Ivan Petřík[3], Yanbiao Sun[1,2], Jonah Nolf[1,2], Wouter Smet[1,2], Kevin Verstaen[4,5], Jos R. Wendrich[1,2], Thomas Eekhout[1,2], Klára Hoyerová[6], Gert Van Isterdael[7,8], Jurgen Haustraete[8,9], Anthony Bishopp[10], Etienne Farcot[11], Ondřej Novák[3], Yvan Saeys[4,5] and Bert De Rybel[1,2]✉

During plant development, a precise balance of cytokinin is crucial for correct growth and patterning, but it remains unclear how this is achieved across different cell types and in the context of a growing organ. Here we show that in the root apical meristem, the TMO5/LHW complex increases active cytokinin levels via two cooperatively acting enzymes. By profiling the transcriptomic changes of increased cytokinin at single-cell level, we further show that this effect is counteracted by a tissue-specific increase in *CYTOKININ OXIDASE 3* expression via direct activation of the mobile transcription factor SHORTROOT. In summary, we show that within the root meristem, xylem cells act as a local organizer of vascular development by non-autonomously regulating cytokinin levels in neighbouring procambium cells via sequential induction and repression modules.

The plant vasculature is a complex tissue composed of multiple cell types, each with a specific function[1]. In the *Arabidopsis* root apical meristem during primary growth, vascular tissues are organized according to a bilateral symmetry, with a central xylem axis flanked by two phloem poles with intervening procambium cells[1,2]. Previous work has shown that this patterning is established and maintained by a domain of high-auxin signalling in the xylem cells and a domain of high-cytokinin signalling in the procambium and phloem cell lineages[3–5], making this an excellent model system to study coordinated development involving intercellular communication, hormonal signalling and crosstalk. On a molecular level, growth and patterning of vascular tissues is in part driven by the heterodimer formed by the basic helix loop helix transcription factors TARGET OF MONOPTEROS 5 and LONESOME HIGHWAY (TMO5/LHW)[6–11]. This complex triggers local biosynthesis of cytokinin via direct activation of LONELY GUY 3 and 4 (LOG3/4)[4,5]. This xylem-derived cytokinin is thought to diffuse to neighbouring procambium cells where it drives vascular proliferation by activating downstream target genes, including members of the DNA-binding-with-one-finger (DOF)-type transcription factor family[12,13]. Although it is clear that TMO5/LHW plays an important role in controlling vascular growth and patterning[4,5], it remains unclear how appropriate cytokinin levels are maintained in each cell type in the context of a growing tissue[14].

BGLU44 and LOG4 cooperatively produce active cytokinin

TMO5/LHW activity is dependent on the phytohormone cytokinin as this dimer is inactive when cytokinin biosynthesis (for example, in a *log1234578* mutant[15,16]) or signalling (for example, in a *wol* mutant[17]) are perturbed[4]. Although *LOG3* and *LOG4* were identified as main target genes of the TMO5/LHW dimer[4,5], misexpression of *LOG* genes does not result in the strong cytokinin-related vascular phenotypes observed upon exogenous cytokinin treatment or TMO5/LHW induction[4], suggesting that additional factors are involved in releasing active cytokinin. To identify such factors, we overlapped genes co-expressed with *LOG4* in a high spatiotemporal resolution single-cell dataset (Fig. 1a, Extended Data Fig. 1 and Supplementary Data 1)[18] with a list of putative TMO5/LHW target genes[13]. The overlap contained the closely related *LOG3*[4,5], the negative regulator of TMO5/LHW activity *SACL3*[7,11] and an uncharacterized beta-glucosidase family member *BGLU44/AT3G18080* (Fig. 1a, Extended Data Fig. 2a–c and Supplementary Data 1). By quantitative reverse transcription–polymerase chain reaction (RT-qPCR) analysis, we found that relative expression levels of *BGLU44* were increased upon TMO5/LHW induction and reduced in *tmo5* single, double and triple mutant backgrounds (Fig. 1b), similar to *LOG4*[4]. We next constructed a p*BGLU44*-nYFP/GUS reporter line and found *BGLU44* expressed in the root apical meristem along the xylem axis and in xylem pole-associated pericycle and endodermis cells as predicted by single-cell RNA-sequencing (scRNA-seq) atlas data[18] (Fig. 1c,d and Extended Data Fig. 2a–c), and its expression patterns identical to those of *LOG4* in this tissue[4]. Induction of the TMO5/LHW heterodimer throughout the root meristem (using a dexamethasone (DEX) double inducible p*RPS5A*::TMO5:GR x p*RPS5A*::LHW:GR or dGR line[13]) triggered both increased and

[1]Department of Plant Biotechnology and Bioinformatics, Ghent University, Ghent, Belgium. [2]VIB Center for Plant Systems Biology, Ghent, Belgium. [3]Laboratory of Growth Regulators, Institute of Experimental Botany of the Czech Academy of Sciences and Faculty of Science of Palacký University, Olomouc, Czech Republic. [4]Department of Applied Mathematics, Computer Science and Statistics, Ghent University, Ghent, Belgium. [5]VIB Center for Inflammation Research, Data Mining and Modelling for Biomedicine, Ghent, Belgium. [6]Laboratory of Hormonal Regulations in Plants, Institute of Experimental Botany, Czech Academy of Sciences, Prague, Czech Republic. [7]VIB Flow Core, VIB Center for Inflammation Research, Ghent, Belgium. [8]Department of Biomedical Molecular Biology, Ghent University, Ghent, Belgium. [9]VIB Protein Service Facility, VIB Center for Inflammation Research, Ghent, Belgium. [10]School of Biosciences, University of Nottingham, Loughborough, UK. [11]School of Mathematical Sciences, University of Nottingham, Nottingham, UK. ✉e-mail: baojun.yang@psb.vib-ugent.be; bert.derybel@psb.vib-ugent.be

ectopic p*BGLU44*::nYFP/GUS expression (Fig. 1e,f and Extended Data Fig. 2d–g), suggesting that BGLU44 acts downstream of TMO5/LHW. By chromatin immunoprecipitation (ChIP)-RT-qPCR analysis, we found a significant binding of TMO5-GR/LHW-GR to the *BGLU44* promoter region, indicating that *BGLU44* is a direct target of TMO5/LHW (Extended Data Fig. 3a). Taken together, these results confirm the TMO5/LHW-dependent co-expression of *BGLU44* and *LOG4*.

BGLU44 encodes a member of the glycoside hydrolase family 1, comprising over 40 members in both *Arabidopsis* and rice[19]. Although BGLU proteins have been implicated in various developmental processes including mobilization of storage compounds[20] and reconstruction of cell walls[21], the beta-glucosidase Zm-p60.1 in maize was shown to cleave biologically inactive cytokinin conjugates to release active cytokinin[22]. To investigate the possibility that BGLU44 would have a similar role in *Arabidopsis*, we misexpressed *BGLU44* from the strong meristematic *RPS5A* promoter[23] (Extended Data Fig. 2h–j) and analysed xylem differentiation in the root as proxy for active cytokinin levels[4]. As positive control, TMO5/LHW misexpression (dGR line) resulted in a loss of protoxylem differentiation compared to the wild type control situation (Fig. 1k,l). We did not observe any differences in the p*RPS5A*::BGLU44 line compared to wild type plants (Fig. 1g,i,l and Extended Data Fig. 2h). Considering that the p*RPS5A*::LOG4 misexpression line shows mild vascular defects in the root meristem[4] (Fig. 1g,h,l), we hypothesized that both enzymes might work in a cooperative manner. We thus combined both misexpression lines via crossing (p*RPS5A*::LOG4 x p*RPS5A*::BGLU44) and observed a defect in silique positioning on the stem (Extended Data Fig. 2h,i) and an increase in root hairs (Extended Data Fig. 2t–w) as also seen in TMO5/LHW-misexpressing[18] and cytokinin-overproducing plants[24]. When analysing the root meristem vascular tissues, we found an almost complete loss of protoxylem differentiation in the root (Fig. 1j–l), phenocopying the higher cytokinin levels found in TMO5/LHW misexpression lines[4]. Fitting with this observation, combined misexpression of *LOG4* and *BGLU44* resulted in a small but significant increase in the number of vascular cell files (Extended Data Fig. 2k–o). Similarly, a newly generated *bglu44* loss-of-function CRISPR line, which led to a large fragment deletion, did not result in a strong phenotype, but enhanced the reduction of vascular cell numbers when combined with *log4* or *log3 log4* mutants (Extended Data Fig. 4), suggesting that LOG4 and BGLU44 play a role in vascular proliferation. To further understand whether increased LOG4 and BGLU44 expression are related to increased levels of active cytokinin, we next analysed the two-component signaling sensor nuclear (TCSn) reporter for cytokinin signalling[13,25] fused to the nuclear tdTomato fluorescent protein (pTCSn::ntdT) in the combined misexpression background. Confocal imaging confirmed that plants overexpressing both *LOG4* and *BGLU44*, but not the individual factors, caused increased expression of TCSn, which was most prominent in the ground tissues that typically show very low TCSn expression in wild-type plants (Fig. 1m–q and Extended Data Fig. 2p–s). Finally, we assayed the enzymatic activity of the BGLU44 protein (Extended Data Fig. 4d). First, we tested specificity of BGLU44 activity in vitro for several glucose-conjugated cytokinin substrates and found that it is specific to O-glucoside cytokinin species (Fig. 1r). Moreover, BGLU44 is able to cleave the inactive conjugated tZOG and tZROG species into the bio-active tZ and tZR (Fig. 1s and Source Data Fig. 1). Measuring the endogenous cytokinin profiles of 7-day-old root tips in LOG4, BGLU44, LOG4/BGLU44 and dGR misexpression lines revealed that the combined misexpression of LOG4 and BGLU44 resulted in a similar increase in cytokinin levels as previously shown for TMO5/LHW[4] (Fig. 1t and Source Data Fig. 1). Taken together, our results show that BGLU44 and LOG4 cooperatively act downstream of TMO5/LHW to release active cytokinin in the vascular bundle of the root meristem, thereby controlling primary vascular development.

CKX3 balances cytokinin levels downstream of TMO5/LHW

Cytokinin levels need to be well balanced in space and time to allow normal development. Indeed, high levels of active cytokinin disturb normal vascular cell proliferation, patterning and differentiation[15,16,26,27] (Fig. 3n). The active cytokinin produced in the central xylem axis, where TMO5/LHW activity overlaps with *LOG4* and *BGLU44* expression, is thought to diffuse to neighbouring procambium and phloem cells[3–5], which show high levels of cytokinin signalling. To understand the tissue-specific responses of increased cytokinin levels, we profiled the transcriptional effect of cytokinin treatment on root meristem cells at single-cell resolution (Fig. 2a,b). After filtering, we retained about 10,000 high quality cells for each sample with a minimal unique molecular identifier (UMI) count of more than 1,000 (Fig. 2a). Clear transcriptional changes were observed for most cell types, while some subpopulations remained largely unaffected, such as the protoxylem and columella cells (Extended Data Fig. 5a–c), suggesting tissue-specific responses. As expected, primary response genes of the cytokinin signalling pathway, such as A-type *ARABIDOPSIS RESPONSE REGULATORS* (*ARR*), were recovered as cytokinin inducible in all cell clusters (Supplementary Data 2). We next created transcriptional reporter lines for 12 genes previously uncharacterized for cytokinin response in the root meristem and showing tissue-specific cytokinin responses. These lines show both the predicted tissue-specific expression pattern in the mock situation and the tissue-specific induction kinetics after cytokinin treatment in the root (Supplementary Fig. 1), thus validating the predictive power of our dataset.

Given that procambium cells are those responding to cytokinin levels with respect to cell proliferation in our system, we next searched our dataset for those genes specifically responding to the

Fig. 1 | *BGLU44* and *LOG4* cooperatively produce active cytokinin downstream of TMO5/LHW. a, Schematic representation of the strategy to identify *BGLU44* as putative target gene of TMO5/LHW. **b**, Relative expression levels of *BGLU44* and *LOG4* in wild type (Col-0), TMO5/LHW misexpression, and *tmo5*, *tmo5 tmo5like1* (*t5 t5l1*) and *tmo5 tmo5like1 tmo5like3* (*t5 t5l1 t5l3*) mutant backgrounds. The coloured lines indicate the median value of three biological replicates ($n = 3$), while the grey area shows the data range (*$P < 0.05$). The dashed black line indicates the expression level of the control sample, which was set to 1. **c**–**f**, Expression of p*BGLU44*::nYFP/GUS in the dGR root meristem grown on mock medium and transferred to mock or 10 µM DEX for 24 h. Asterisks indicate the endodermis cell layer. **g**–**k**, Microscopic images of xylem differentiation in the mentioned genotypes. p, protoxylem; m, metaxylem. **l**, Quantification of the different classes of xylem phenotypes shown in panels **g**–**k**. **m**–**p**, Confocal images of root meristems expressing pTCSn::ntdTomato reporter in the mentioned genotypes. Arrows in **p** indicate cortex cell layer. **q**, Quantification of the pTCSn::ntdTomato mean pixel intensity in the mentioned genotypes. Boxes represent the 1st and 3rd quartiles, and the centre line represents the median. **r**, In vitro BGLU44 enzymatic activity on a range of cytokinin glycoside substrates. **s**, In vitro cleavage of O-glucosylated cytokinins by BGLU44. **t**, Overview of total endogenous cytokinin levels in root tips of the indicated lines. Lowercase letters in graphs indicate significantly different groups as determined by one-way ANOVA with post-hoc Tukey HSD testing ($P < 0.001$). Asterisks in graphs indicate significance values as determined by standard two-sided *t*-tests. Coloured lines indicate mean values and grey boxes indicate data ranges. Scale bars in **c**–**k** and **m**–**p**, 50 µm. In all panels, *n* represents the number of replicates or data points; all data and statistics are summarized in Source Data Fig. 1. The experiments in **c**–**f** were repeated three times independently, with similar results.

increase in cytokinin levels in the procambium cell cluster only. We found that among the top candidates, *CYTOKININ OXIDASE3* (*CKX3/AT5G56970*) was recovered as specifically induced by cytokinin in procambium cells (Fig. 2c,d and Supplementary Data 2). As CKX proteins have been shown to reduce levels of active cytokinin[24,26,28], CKX3 could be the factor that counteracts the flow of active cytokinin from the xylem cells and ensure well-balanced cytokinin levels. Indeed, previous reports suggested that cytokinin could balance itself by promoting cytokinin oxidase expression[29,30]. We confirmed the cytokinin inducibility of *CKX3* in procambium cells by generating a p*CKX3*::nYFP-GUS transcriptional reporter using a 4.2 kb promoter fragment (Fig. 2e,f). Upon transfer to 10 µM 6-benzylaminopurine (BAP) for 3 h, a significant increase in *CKX3* expression levels in procambium cells was observed (Fig. 2g–i) as predicted by the scRNA-seq dataset (Fig. 2c,d and Extended Data Fig. 5e).

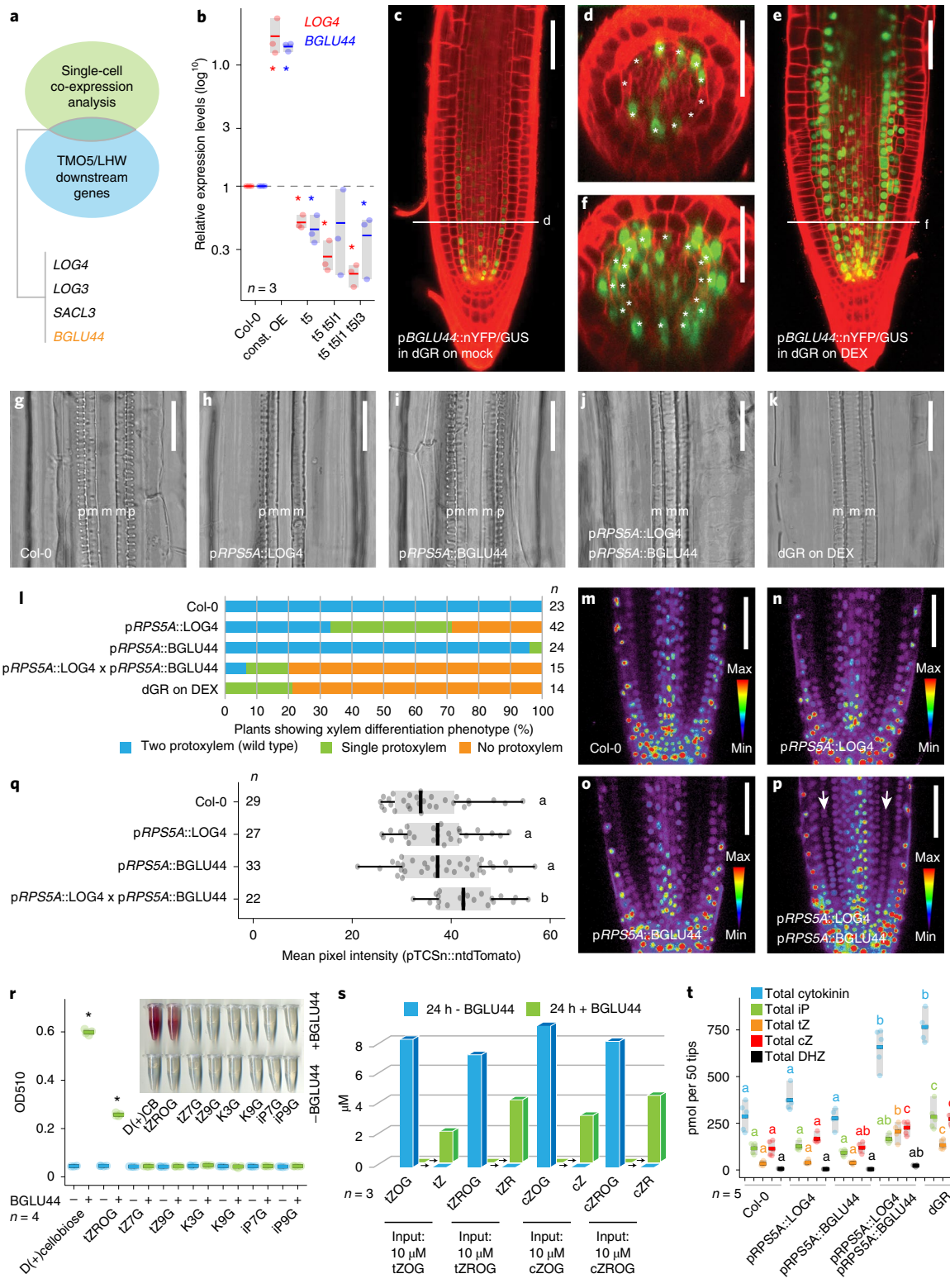

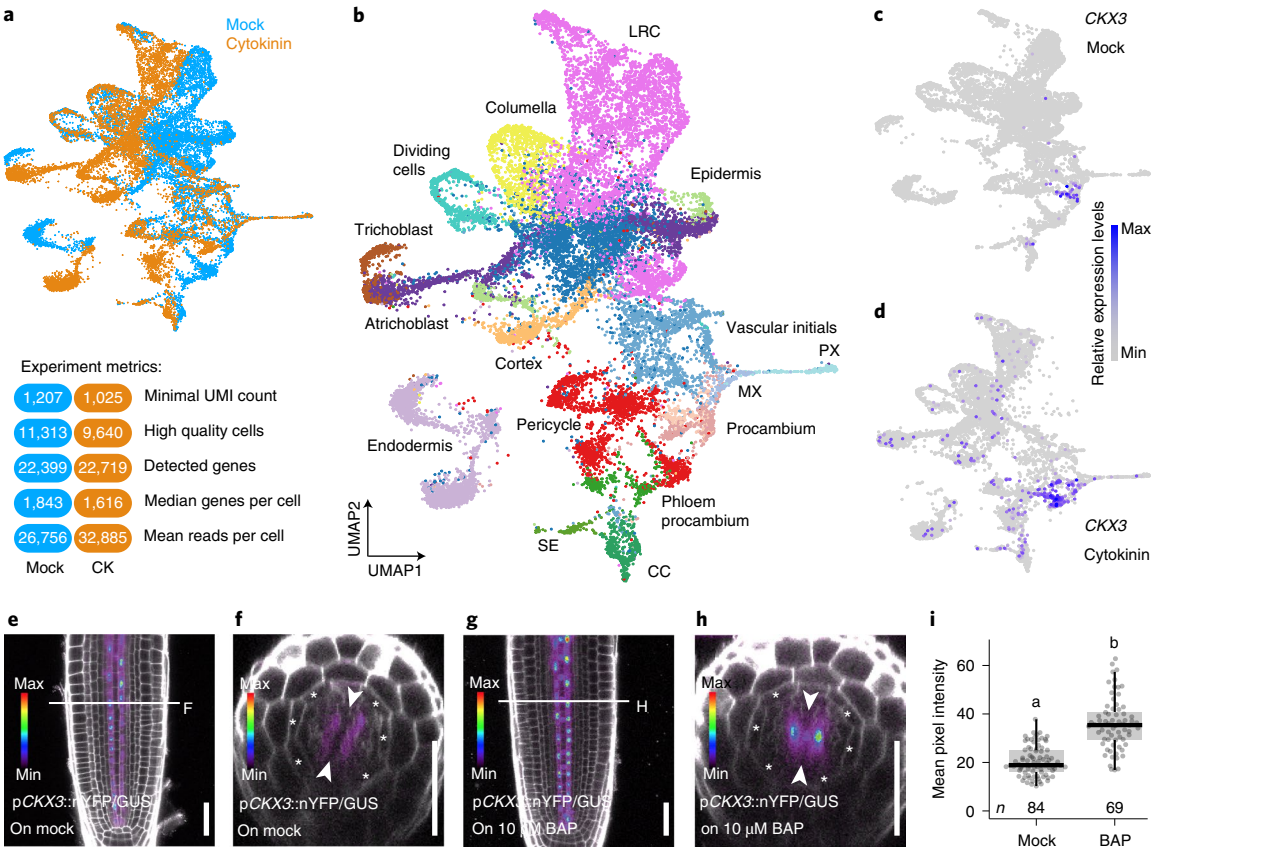

Fig. 2 | Single-cell transcriptional changes in root meristem cells upon cytokinin treatment. a, Uniform Manifold Approximation and Projection (UMAP) plot showing the merge of the mock and cytokinin samples, and an overview of the experimental metrics for both samples. **b**, UMAP plot of the merged data with indications of the different cell identities. LRC, lateral root cap; PX, protoxylem; MX, metaxylem; SE, sieve element; CC, companion cell. The most central dark blue cell cluster is the initial cell cluster. **c**,**d**, Feature plots of *CKX3* expression in the mock (**c**) and cytokinin (**d**) datasets showing a tissue-specific induction in the procambium cells. **e**–**h**, Expression of p*CKX3*::nYFP/GUS in the root meristem grown on mock medium and transferred to mock or 10 µM BAP for 3 h. Asterisks indicate the endodermis cell layer. Arrowheads indicate xylem axis. Scale bars, 50 µm. **i**, Quantification of the experiment described in **e**–**h**. Lowercase letters on top of the boxplots indicate significantly different groups as determined by one-way ANOVA with post-hoc Tukey HSD testing ($P < 0.001$). Boxes represent the 1st and 3rd quartiles, and the centre line represents the median. In all panels, *n* represents the number of replicates or data points; all data and statistics are summarized in Source Data Fig. 2.

To further understand whether the *CKX3* regulation by cytokinin is related to TMO5/LHW, we first confirmed by RT-qPCR that relative expression levels are increased upon induction of the TMO5/LHW heterodimer and downregulated in *tmo5* double and triple mutants (Fig. 3a), providing support that CKX3 indeed acts downstream of TMO5/LHW. We next introduced the transcriptional p*CKX3*::nYFP/GUS line (Fig. 3b–e) and a newly generated translational p*CKX3*::CKX3:GFP reporter line (Fig. 3f–i) in the dGR background. Upon misexpression of TMO5/LHW, expression of *CKX3* increased and now marked the entire vascular cylinder (Fig. 3d,e,h,i). To further assess a possible role for CKX3 during vascular development, we analysed phenotypes upon loss of function of CKX3 and its close homologue CKX5, which shows a similar expression pattern as predicted by our scRNA-seq dataset (Extended Data Figs. 5f and 6a,b) and validated by a newly generated 3.5 kb p*CKX5*::nYFP/GUS reporter line (Extended Data Fig. 6c,d). The *ckx3 ckx5* double mutant[24], but not the *ckx3* or *ckx5* single mutants, showed additional metaxylem cell files in over 60% of plants analysed (Extended Data Fig. 6e–h,l) and vascular cell file number was increased (Extended Data Fig. 6m–q). This is opposite to the effect of reducing cytokinin biosynthesis in *log* higher-order mutants (Extended Data Fig. 6i–l)[4,16]. These results suggest that CKX3 (in collaboration with CKX5) is involved in modulating vascular cytokinin levels. To further investigate the importance of CKX3 function downstream of TMO5/LHW, we generated p*RPS5A*::CKX3:YFP misexpression lines in the dGR background. Unlike the dGR control situation where DEX treatment inhibited protoxylem differentiation (Fig. 3j,k,o) and increased vascular cell file number (Fig. 3p,q,t)[6], CKX3 misexpression completely repressed TMO5/LHW function (Fig. 3l,m,o,r–t). These results show that TMO5/LHW not only promotes release of active cytokinin via LOG4 and BGLU44, but at the same time represses active cytokinin in procambium cells via CKX3 to maintain optimal levels of cytokinin for normal vascular development. To further examine the importance of TMO5/LHW in CKX3 regulation, we treated wild type and *tmo5* triple mutants with exogenous cytokinin. While cytokinin increased relative expression levels of *CKX3* in a wild-type Col-0 background, this response was repressed in the absence of TMO5 activity (Extended Data Fig. 6r), suggesting that TMO5/LHW is an important regulator of *CKX3* expression. Considering that *TMO5* and *CKX3* expression domains are in neighbouring cell types, we hypothesize that there must be a mobile intermediate connecting these two factors.

SHR bridges TMO5/LHW-dependent regulation of *CKX3* expression

The mobile transcription factor SHORT-ROOT (SHR) has been shown to directly bind to the *CKX3* promoter region and regulate its expression levels[31]. Although cytokinin levels[31] and signalling

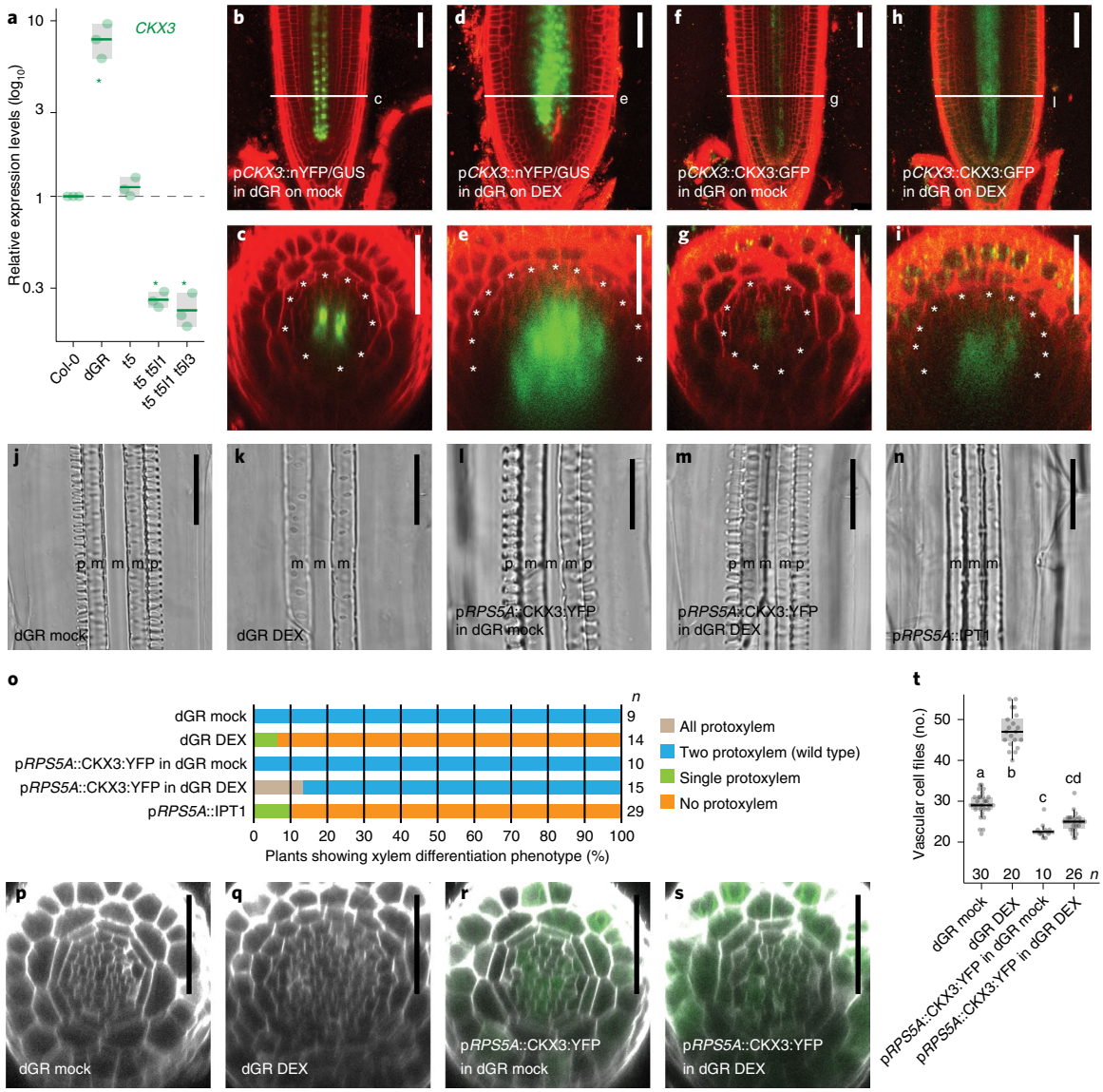

Fig. 3 | CKX3 balances cytokinin levels downstream of TMO5/LHW. a, Relative expression levels of *CKX3* in wild type (Col-0), TMO5/LHW misexpression, and *tmo5, tmo5 tmo5like1* (*t5 t5l1*) and *tmo5 tmo5like1 tmo5like3* (*t5 t5l1 t5l3*) mutant backgrounds. Boxes represent the 1st and 3rd quartiles, and the centre line represents the median. $n = 3$ biological replicates ($^*P < 0.05$). The dashed black line indicates the expression level of the control sample, which was set to 1. **b–i**, Expression of p*CKX3*::nYFP/GUS and p*CKX3*::CKX3:GFP in the dGR root meristem grown on mock medium and transferred to mock or 10 µM DEX for 24 h. Asterisks indicate the endodermis cell layer. **j–n**, Microscopy images of xylem differentiation in the mentioned genotypes. p, protoxylem; m, metaxylem. **o**, Quantification of the different classes of xylem phenotypes shown in **j–n**. **p–s**, Confocal cross-section images through the root meristem of the mentioned genotypes grown on mock medium and transferred to mock or 10 µM DEX for 24 h. **t**, Quantification of the number of vascular cell files shown in **p–s**. Lowercase letters on top of the boxplots indicate significantly different groups as determined by one-way ANOVA with post-hoc Tukey HSD testing ($P < 0.001$). Boxes represent the 1st and 3rd quartiles, and the centre line represents the median. Asterisks in graphs indicate significance values as determined by standard two-sided *t*-tests. Black lines indicate mean values and grey boxes indicate data ranges. Scale bars in **b–n** and **p–s**, 50 µm. In all panels, *n* represents the number of replicates or data points; all data and statistics are summarized in Source Data Fig. 3. The experiments in **b–i** were repeated three times independently, with similar results.

(Extended Data Fig. 7a–c) are high in a *shr-2* mutant background, *CKX3* expression levels are reduced[31]. This suggests that although *CKX3* expression levels can be controlled by cytokinin and SHR, both of which are mobile in the vascular tissues, the dominant form of regulation acts via SHR. To explore the importance of SHR in the connection between TMO5/LHW and CKX3 regulation during vascular development, we first introduced a p*SHR*::SHR:GFP translational reporter line in dGR plants. Upon induction of TMO5/LHW by DEX treatment, the SHR:GFP fusion protein was ectopically present throughout the root meristem (Extended Data Fig. 7d–g). To understand if this was caused by regulation at the transcriptional level, we next introduced a p*SHR*::nYFP/GUS transcriptional reporter line in dGR. Also in this case, induction of TMO5/LHW caused ectopic expression of *SHR* throughout the root meristem (Fig. 4a–d), suggesting that TMO5/LHW might control *SHR* expression. These results were further supported by RT-qPCR data showing that relative expression levels of *SHR* were increased in a TMO5/LHW heterodimer misexpression line and repressed in *tmo5* higher order mutant lines (Extended Data Fig. 7h). To evaluate whether TMO5/LHW directly activates *SHR*

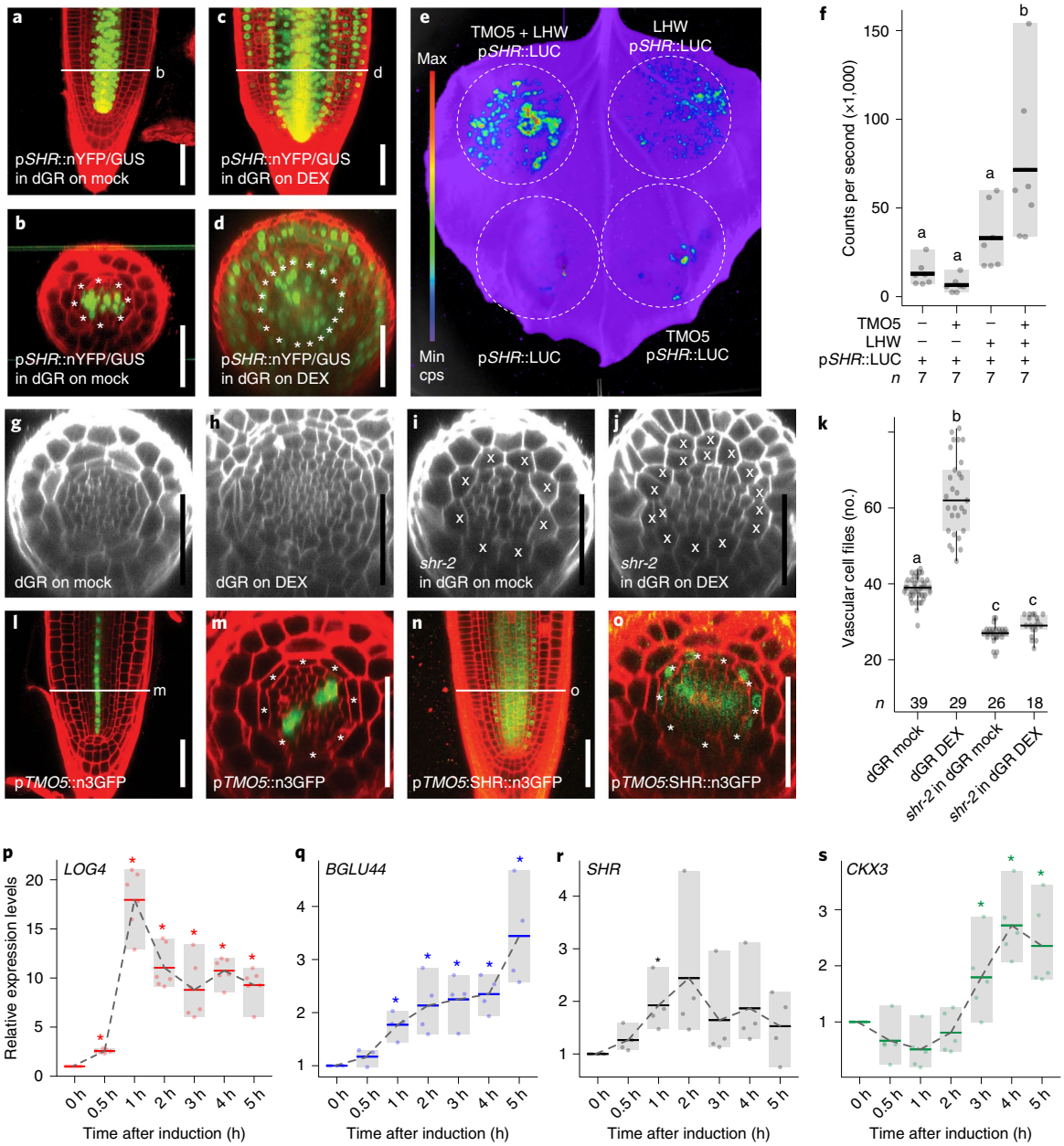

Fig. 4 | SHR bridges TMO5/LHW-dependent regulation of *CKX3* expression. a–d, Expression of p*SHR*::nYFP/GUS in the dGR root meristem grown on mock medium and transferred to mock or 10 µM DEX for 24 h. Asterisks indicate the endodermis cell layer. **e**,**f**, Transient luciferase assay in tobacco leaves showing p*SHR*::LUC expression in the mentioned combination of introduced constructs. Boxes represent the 1st and 3rd quartiles, and the centre line represents the median. $n = 7$ independent tobacco leaves. **g–j**, Confocal cross-section images through the root meristem of the mentioned genotypes grown on mock medium and transferred to mock or 10 µM DEX for 24 h. **k**, Quantification of the number of vascular and endodermis cell files shown in panels **g–j**. The x in **i** and **j** indicates cells with mixed cortex–endodermis identity in the *shr-2* mutant. Boxes represent the 1st and 3rd quartiles, and the centre line represents the median. **l–o**, Expression of p*TMO5*::n3GFP (**l**,**m**) and p*TMO5*::SHR:GFP (**n**,**o**) in the root meristem grown on mock medium. **p–s**, Relative expression levels of *LOG4*, *BGLU44*, *SHR* and *CKX3* in dGR grown on mock and transferred to 10 µM DEX for the indicated time before sampling. Lowercase letters on top of the graphs indicate significantly different groups as determined by one-way ANOVA with post-hoc Tukey HSD testing ($P < 0.001$). Boxes represent the 1st and 3rd quartiles, and the centre line represents the median. $n = 4$–6 biological replicates. Asterisks in graphs indicate significance values as determined by standard two-sided *t*-tests ($^*P < 0.05$). Coloured lines indicate mean values and grey boxes indicate data ranges. In all panels, *n* represents the number of replicates or data points; all data and statistics are summarized in Source Data Fig. 4. The experiments in **a–d** and **i–o** were repeated three times independently, with similar results.

expression, we fused a 2.5 kb promoter fragment of *SHR*[32] to luciferase and introduced this construct in tobacco leaves in the presence of TMO5/LHW. p*SHR*::LUC was induced by TMO5/LHW, while this was not the case in the negative controls and not significantly different in the presence of the individual members of the dimer (Fig. 4e,f), fitting with the previous findings that TMO5 and LHW act as an obligate heterodimer[6,9]. These results were confirmed by ChIP-RT-qPCR (Extended Data Fig. 3b). Taken together, these results suggest that TMO5/LHW directly binds to the *SHR* promoter region to activate its expression.

To further study the genetic relationship between SHR and the TMO5/LHW heterodimer complex, we introduced the *shr-2* mutation[33] into a dGR background by crossing. Although some periclinal divisions were still observed, vascular cell file numbers were not significantly increased in the presence of the *shr-2* mutation (Fig. 4g–k), suggesting that SHR is required for normal TMO5/LHW function. We observed a loss of protoxylem differentiation in *shr-2*, both with and without induction of dGR (Extended Data Fig. 7i–m), in line with the high cytokinin levels in this mutant background[31]. Moreover, we found that xylem-expressed SHR (p*TMO5*::SHR:GFP) is capable of moving throughout the vascular bundle (Fig. 4l–o), and is capable of rescuing the *shr-2* root length and ground tissue cell identity phenotypes in a dose-dependent manner (Extended Data Fig. 8). This indicates that TMO5/LHW-driven SHR protein can move from xylem cells into adjacent procambium cells to regulate *CKX3* expression, thereby balancing overall cytokinin levels. The relevance of TMO5/LHW regulation on the extended SHR transcriptional pathway was further highlighted by the fact that also its interactor SCARECROW and downstream target miRNA165 are controlled by TMO5/LHW activity (Extended Data Fig. 7n–s). As such, the xylem axis works as a central organizer for vascular development and patterning via SHR.

Spatiotemporal regulation of vascular cytokinin levels

Our results suggest that downstream of TMO5/LHW, the LOG4 and BGLU44 enzymes cooperatively work to increase levels of active cytokinin in the xylem axis, while CKX3 reduces cytokinin levels in the neighbouring procambium cells via SHR as a mobile intermediate, and independent of cytokinin signalling. These results are in line with the hypothesis that the xylem axis acts as an insensitive source of active cytokinin, which is thought to diffuse to the neighbouring procambium cells[4,5]. In the procambium domain, cells are responsive to cytokinin[3,4,17,27] and thus require a repressive mechanism to cope with the influx of active cytokinin and obtain optimal levels for normal development. We next questioned whether these different factors responsible for the increase and decrease of active cytokinin levels are activated simultaneously or in sequence. By analysing the temporal changes in expression levels via RT-qPCR, we show that *LOG4* is increased in expression levels around 30 min to 1 h after TMO5/LHW induction (Fig. 4p), quickly followed by *BGLU44* induction starting around 1 h after TMO5/LHW induction (Fig. 4q). *SHR* expression levels are also induced from 1 h onwards (Fig. 4r), leading to the induction of *CKX3* as a direct SHR target at 3 h after induction (Fig. 4s). A similar trend was observed when analysing the transcriptional reporter lines for *LOG4*, *BGLU44* and *SHR*, and a protein fusion reporter for *CKX3* genes (Supplementary Figs. 2a–c and 3), further corroborating that induction of active cytokinin levels via LOG4 and BGLU44, and repression via SHR and CKX3 are sequential events upon TMO5/LHW induction. Previous mathematical models[4,34] had predicted a network that was conceptually sufficient to determine the correct position of auxin response around an initial asymmetry in cellular pattern. However, these models considered only a fixed basal rate of auxin synthesis, and did not consider how robust this output would be in regards to fluctuations in auxin input. To better understand the spatiotemporal wiring of this network, we generated a mathematical model comprising these molecular players in their respective cells (for a detailed description, see Supplementary Methods: Mathematical Modelling), with auxin signalling as input to TMO5/LHW and cytokinin signalling as output. This model was based around a simplified tissue geometry, but considered fluctuations in the auxin signalling input over time. In the model, the wiring of activation and repression modules is capable of dampening fast oscillating auxin inputs into a continuous cytokinin response, while remaining responsive to slower changes in auxin (Model Description). This response was not dependent on the amplitude of the auxin signalling input, meaning that both small and large changes have an impact on the cytokinin signalling output as long as the frequency of the modulation is low (Model Description).

In conclusion, our findings point to a tight spatiotemporal regulation of cytokinin levels via sequential induction and repression modules, all originating from the same bHLH heterodimer complex (Extended Data Fig. 9). As such, we found that a single transcription factor complex controls multiple biosynthesis and degradation steps of a phytohormone to regulate tissue development in space and time. The fact that these modules with opposite function are initiated as direct targets of the TMO5/LHW complex suggests that cytokinin levels might be balanced without the need for intermediate sensing via canonical CRE1/AHK4/WOL receptor signalling[17,35]. Rather, differences in spatiotemporal activity of these modules might be sufficient to control levels of active cytokinin in the respective tissues and drive the observed self-organizing capacities of vascular patterning and growth[4,34,36]. Intriguingly, our modelling efforts suggest that these cytokinin signalling-controlled processes would not be influenced by fast fluctuations in auxin signalling in the root apical meristem. Rather, vascular patterning and growth controlled by the TMO5/LHW dimer would be sensitive to slow and gradual changes in the auxin input. Although additional experimental work is required to support this hypothesis, this emerging property of the model makes sense in the context of a growing tissue where growth and patterning respond to gradual modulation of hormone levels. Our work also identifies the central xylem cells as a tissue organizer for vascular development and highlights TMO5/LHW as upstream regulator of SHR, a central transcriptional hub controlling several distinct aspects of growth and development in vascular and other tissues[33,37–39]. Given that MONOPTEROS was previously shown to control SHR expression[40], it is conceivable that within the context of vascular development this regulation is indirect and requires TMO5 as an intermediate factor. It remains to be determined if and how TMO5/LHW would be connected to other SHR-controlled processes during plant development.

Methods

Plant materials and growth condition. *Arabidopsis thaliana* ecotype Columbia-0 (Col-0) was used in all transformation and phenotype analysis. All seeds were germinated on ½MS (Murashige and Skoog, Duchefa) medium after 3 d stratification at 4 °C. Seedlings and plants were grown at 22 °C in continuous light conditions. Glucocorticoid receptor (GR)-related inducible plants (7 days old) were transferred from 1/2 MS to 10 µM DEX-supplemented medium and allowed to grow for the indicated time. Plant lines and mutants used in this study are dGR[13], p*SHR*::SHR:GFP[38], pTCSn::ntdTomato[13], p*RPS5A*::LOG4[4], *ckx3*[24], *ckx5*[24], *ckx3 ckx5*[24], *log4*[16], *log3 log4*[16], *log3 log4 log7*[16], *shr-2*[33], *tmo5*[6], *tmo5t 5l1*[6] and *tmo5 t5l1 t5l3*[6]. The Arabidopsis Genome Initiative identifiers for the genes used in this study are as follows: *TMO5*, AT3G25710; *LHW*, AT2G27230; *LOG4*, AT3G53450; *BGLU44*, AT3G18080; *CKX3*, AT5G56970; *CKX5*, AT1G75450; and *SHR*, AT4G37650.

***LOG4*-based single-cell co-expression analysis.** We identified potential co-expressed genes of *LOG4* by computing the Pearson correlation coefficient on the log-normalized UMI counts from a previously published scRNA-seq dataset[18]. Results were next sorted from high to low correlation and the top 50 genes were extracted for further analysis.

Constructions and transformation. All the constructs were generated on the basis of the Multisite Gateway system (Invitrogen)[41]. To generate transcriptional reporters, up to 4 kb promoters amplified using Col-0 genomic DNA as template were cloned into pDONRP4P1R entry vectors by BP reaction (see detailed information in Supplementary Data 3). The entry vectors containing the promoter regions were next recombined into the binary vector pH7m34GW along with pDONR221-nYFP and pDONRP2RP3-GUS. Protein fusion reporters were obtained by cloning the respective promoter fragments into pDONRP4P1R, the respective coding sequence without stop codon into the entry clone pDONR221, and a fluorescence tag (GFP or YFP) into pH7m34GW destination vector using Gateway cloning. To generate the luciferase (LUC) expression vector, coding sequences of the transcription factors TMO5 and LHW were cloned into the pDONR221 entry vector using the BP clonase system. The CaMV35S constitutive promoter (35S) fused to these transcription factors were generated via an LR clonase reaction with the pH7FWG2.0 vector. Promoter fragments of *LOG4* were

cloned into pDONRP4P1R. A promoter fragment fused to the luciferase reporter gene was developed by the two-fragment gateway system with pDONR221-LUC and pH7m24GW.3. All constructs were verified by Sanger sequencing and were transformed into wild-type Col-0 or the dGR[13] *Arabidopsis* plants using floral dipping. All primer sequences used for cloning and sequencing are listed in Supplementary Data 3. The resulting constructs were transformed into *Agrobacterium tumefaciens* strain GV3101.

BGLU44 CRISPR mutant generation. Four guide RNAs (gRNAs) were designed for targeting BGLU44 using the CRISPR-P tool[42]. Cloning of gRNA vectors was performed essentially as previously described[13]. Oligos were annealed and ligated into six Golden Gate gRNA entry modules using standard DNA ligation and the sequences verified. The gRNA entry plasmids were cloned into the pFASTRK_AtCas9_AG destination vector (https://gateway.psb.ugent.be) using Golden Gate assembly. Plants were transformed with *Agrobacterium* cultures using floral dip. A positive transgene was selected by red seed fluorescence. Deletion mutations in the target gene were confirmed in the T1 generation by PCR amplification and sequencing. T3 Cas9-free, homozygous knockout plants were selected and used for phenotype analysis. To generate *bglu44 log4* or *bglu44 log3 log4* triple mutants, homozygous *bglu44* mutants was crossed with *log4* or *log3 log4* mutants and homozygous seeds were identified by PCR. Primers used for PCR and sequencing can be found in Supplementary Data 3, *log3* and *log4* mutants identification primers were used as previously described[15].

Imaging and processing. Xylem differentiation was observed using differential interference contrast (DIC) microscopy by mounting samples in a solution of 20% glycerol and 60% lactic acid, and imaged using an Olympus BX53 microscope equipped with DIC optics[4]. GUS staining of the p*BGLU44*::nYFP-GUS was performed using GUS staining methods[43]. Cell wall staining for optical confocal cross sections was done using the ClearSee protocol including cell wall staining with 0.1% Calcofluor White[44]. Confocal laser scanning microscopy was performed using a Leica SP8X device with 40X water-corrected objectives (NA 1.2) using an argon laser excitation wavelength of 405 nm for Calcofluor White, 488 nm for GFP, 514 nm for YFP and 561 nm for nuclear tdTomato (tdT)- and propium iodide (PI)-stained samples. Calcofluor White, GFP, YFP, tdT and PI were visualized at an emission of 425–475 nm, 500–535 nm, 520–550 nm, 580–630 nm and 600–700 nm, respectively. Images were then processed using Leica Application Suit X. All optical cross sections were made in the middle of the meristem, determined by the quiescent center on one end and the first elongating cortex cell on the other end. The vascular cell file numbers were also counted in this position.

RNA extraction and qRT-PCR analysis. Total RNAs were extracted from 7-day-old seedling roots using Trizol reagent (Invitrogen) with RNeasy Kit (QIAGEN) as previously described[43] and reversely transcribed to first-strand complementary DNA by qScript cDNA SuperMix (QUANTABIO). qRT-PCR analysis was performed with SYBR GREEN I Master kit (Roche) and data were collected on a LightCycler480 apparatus (Roche) detection system in accordance with the manufacturer's instructions. Data analysis was performed with Q-Base+[45] and transcript levels were normalized to EEF1a4 and CDKA1;1. All qRT-PCR primers used in this study are listed in Supplementary Data 3.

Transient expression in *Nicotiana benthamiana* and LUC assay. *A. tumefaciens* strains GV3101 carrying expression constructs (p*35S*::TMO5, p*35S*::LHW and p*SHR*::LUC) were grown in YEP media overnight, centrifuged and resuspended in infiltration buffer (10 mM MES, 10 mM MgCl2 and 200 µM acetosyringone) at OD_{600} 1.0. Equal volumes of cultures of different constructs were mixed for infiltration. To prevent gene silencing, p19 agrobacterial culture was mixed with the combinations. Cultures were then spot-infiltrated into 4-week-old *N. benthamiana* (tobacco) leaves. After 3 d, leaves were cut and sprayed with 1 mM luciferin, which were then imaged for an 11 min exposure using a NightSHADE LB 985 system (Berthold Technologies).

Chromatin immunoprecipitation (ChIP). ChIP was performed using universal plant ChIP kit (C01010152, Diagenode). One gram roots of 7-day-old dGR and Col-0 seedlings transferred to MS medium with DEX for 24 h were used. Anti-GR antibody (PA1-516, Invitrogen) was bound to Protein A Dynabeads (Diagenode) and incubated with chromatin sample overnight at 4 °C. Quantitative PCR reactions of the samples were performed using SYBR GREEN I Master kit (Roche), with the following PCR conditions: 3 min at 95 °C, followed by 45 cycles of 30 s at 95 °C, 30 s at 58 °C and 30 s at 72 °C. Primers used in this study are listed in Supplementary Data 3, SHR ChIP primers were used as previously described[46]. Data were analysed by fold enrichment method (fold enrichment = $2^{-(Ct(Sample)-Ct(Control))}$). Two independent biological replicates were performed.

Protein expression and purification. Mature BGLU44 without signal peptide (AA 24-512) was picked up from a cDNA library, with primers listed in Supplementary Data 3. The PCR fragment was cloned between the SphI and XhoI sites in the linearized ppSA-Ht plasmid (a derivative of the pPICZalphaB vector; provided by the VIB Protein Core) using the Gibson assembly protocol from New England Biolabs. The gene of interest was cloned in the frame of the alpha mating factor for secreted expression. The obtained plasmid was then PmeI-linearized and transformed into NRRL Y-11430 wild-type Komagataella phaffii yeast expression strain. Transformed cells where plated on increasing zeocin concentrations (100 µg ml^{-1}, 250 µg ml^{-1}, 500 µg ml^{-1} and 1,000 µg ml^{-1}) to screen for high-expressing colonies.

Purification was performed according to the method described in ref. [19]. Briefly, biomass was grown by inoculating 250 ml buffered glycerol-complex medium with NRRL Y-11430(ppSA-HT_BGLU44) and incubating for 48 h at 30 °C and 200 r.p.m. Cells where collected by centrifuging for 10 min at 1,500 *g* and resuspended in buffered methanol-complex medium containing 1% MeOH to induce protein expression. Resuspended cultures were grown for 48 h at 30 °C and 200 r.p.m. and spiked with 1% MeOH every 12 h. Cells where pelleted by centrifuging the culture for 10 min at 1,500 *g*. Supernatant was collected and further processed. Diafiltration was performed to transfer the supernatant to 20 mM sodium acetate buffer (pH 5.5). The desalted supernatant was applied to a 5 ml Source 15S cation exchange column (Cytiva) pre-equilibrated with 20 mM sodium acetate buffer (pH 5.5). The column was washed with 20 column volumes of 20 mM sodium acetate buffer (pH 5.5) containing 200 mM NaCl. Protein was eluted with a linear gradient of 20–60% over 10 column volumes with 20 mM sodium acetate buffer supplemented with 1M NaCl (pH 5.5). Fractions with proteins running on the correct molecular weight on an SDS-page gel were then collected and pooled together, and briefly concentrated to 4 ml with an Amicon ultra concentrator with 30 kDa cut-off (Millipore). The concentrate was then loaded and run on a Superdex 200 prep grade column (Cytiva) pre-equilibrated with 20 mM MES (pH 6.0). Fractions containing protein of the correct size were pooled and the concentration was determined using a Trinean dropsense 16 device (Unchained Labs).

BGLU44 enzyme activity (D-glucose method). To determine hydrolase activity towards all cytokinin glycoside substrates, 10 ug BGLU44 was incubated for 2 h at 30 °C in 50 µl assays that contained 200 µg substrate and 100 mM Na_2HPO_4/citric acid buffer (pH 4.5). After terminating the reaction by boiling for 2 min, liberated glucose was determined by the D-glucose assay kit (GOPOD Format, Megazyme). D(+)cellobiose was used as a positive control. All assays were performed in quadruplicate. All cytokinin glycoside substrates used (trans-zeatin-*O*-glucoside riboside, tZROG; trans-zeatin-7-glucoside, tZ7G; trans-zeatin-9-glucoside, tZ9G; kinetin-3-glucoside, K3G; kinetin-9-glucoside, K9G; N6-isspentenyladenine-7-glucoside, iP7G; and N6-isopentenyladenine-9-glucoside, iP9G) were obtained from OlChemIm (Olomouc). Stock solutions were prepared as 50 µg µl^{-1} in dimethylsulfoxide (DMSO; Sigma-Aldrich).

BGLU44 enzymatic assay (MS/MS method). Enzymatic reaction was carried out by incubating 5 uM purified BGLU44 with 10 µM tZOG, tZROG, cZOG or cZROG in Na_2HPO_4/citric acid buffer (pH 4.5) at 30 °C for 30 min, 1 h, 6 h, 12 h and 24 h. Enzymatic reactions were repeated in triplicate and stopped with equal volume of 100% MeOH. The supernatant fractions (2 µl per sample) were then transferred in insert-equipped vials and diluted in 5% (v/v) methanol up to 40 µl. Samples (1 µl) were further injected onto a reversed-phase column (Acquity UPLC BEH Shield RP18 column; 150 × 2.1 mm, 1.7 µm; Waters). Separation was performed on an Acquity UPLC System (Waters). The effluent was introduced into the electrospray ion source of a triple quadrupole mass spectrometer Xevo TQ-S MS (Waters) and analysed according to the UHPLC–ESI–MS/MS method for cytokinin metabolic profiling as described in ref. [47].

Measurements of endogenous cytokinins. Quantification of cytokinin metabolites was performed according to the method described by ref. [47]. Samples (50 pieces of 1 cm root tips) were homogenized and extracted in 0.5 ml modified Bieleski buffer (60% MeOH, 10% HCOOH and 30% H_2O) together with a cocktail of stable isotope-labelled internal standards (0.25 pmol of cytokinin bases, ribosides, *N*-glucosides and 0.5 pmol of cytokinin *O*-glucoside nucleotides per sample added). The extracts were purified using the in-tip microSPE on the basis of the StageTips technology[48]. Briefly, combined multi-StageTips (containing C18/SDB-RPSS/cation-SR layers) were activated sequentially with 50 µl each of acetone, methanol, water, 50% (v/v) nitric acid and water (by centrifugation at 434 *g*, 15 min, 4 °C). After application of the sample (500 µl, 678 *g*, 30 min, 4 °C), the microcolumns were washed sequentially with 50 µl of water and methanol (525 *g*, 20 min, 4 °C), and elution of samples was performed with 50 µl of 0.5 M NH_4OH in 60% (v/v) methanol (525 *g*, 20 min, 4 °C). The eluates were then evaporated to dryness in vacuo and stored at −20 °C. Cytokinin levels were determined using ultra high performance liquid chromatography–electrospray tandem mass spectrometry (UHPLC–MS/MS). Quantification was performed by Masslynx software using a standard isotope dilution method[49]. Five independent biological replicates were performed.

scRNA-seq: protoplasting conditions and FACS. Briefly, 6-day-old seedlings were transferred to 10 µM BAP-supplemented medium or an equal volume of DMSO as mock treatment and allowed to grow for 2 h. The root tips were then cut and incubated in protoplasting Solution B (1.5% (wt/vol) cellulysin and 0.1% (wt/vol) pectolyase in Solution A (600 mM mannitol, 2 mM $MgCl_2$, 0.1% (wt/vol) bovine

serum albumin, 2 mM $CaCl_2$, 2 mM MES, 10 mM KCl, pH 5.5)) for approximately 1 h at room temperature. Cells were filtered through a 70 µm cell strainer and spun down at 200 *g* for 6 min, resuspended in Solution A, filtered through a 40 µm cell strainer and stained for live/dead using 4′,6-diamidino-2-phenylindole (DAPI) at 14 µM final concentration. Cells were sorted on a BD Aria II and protoplasts without the DAPI signal were selected for further analysis.

scRNA-seq: 10X genomics sample preparation, library construction and sequencing. Sorted cells were centrifuged at 400 *g* at 4 °C and resuspended in Solution A to yield an estimated concentration of 1,000 cells per µl. Cellular suspensions were loaded on a Chromium Single Cell 3′ GEM, Library & Gel Bead Kit (V3 chemistry, 10X Genomics) according to the manufacturer's instructions. Sequencing libraries were loaded on an Illumina HiSeq4000 and sequenced following recommendations of 10X genomics at the VIB Nucleomics Core (VIB, Leuven).

scRNA-seq: raw data processing and generation of gene expression matrix. Demultiplexing of the raw sequencing data was done by the 10x CellRanger (version 3.1.0) software 'cellranger mkfastq', which wraps Illumina's bcl2fastq. The fastq files obtained after demultiplexing were used as input for 'cellranger count', which aligns the reads to the *Arabidopsis thaliana* reference genome (Ensemble TAIR10.40) using STAR and collapses them to UMI counts. The result is a large digital expression matrix, with cell barcodes as rows and gene identities as columns. Initial filtering in CellRanger recovered 11,569 cells for the mock-treated sample and 9,799 cells for the cytokinin-treated sample. To ensure that we only used high-quality cells for further analysis, we used the filtered data provided by cellranger. This corresponds to 26,756 mean reads per cell in the mock-treated sample and 32,885 mean reads per cell in the cytokinin-treated sample.

scRNA-seq: data analysis (clustering, identity assignment, differential gene expression and quality control). All analyses were performed in R (version 3.6.0). Pre-processing of the data was done by the scater package (version 1.10.1) according to the workflow proposed by the Marioni lab[50]. Outlier cells were identified on the basis of 2 metrics (library size and number of expressed genes) and were tagged as outliers when they were 4 median absolute deviations away from the median value of these metrics across all cells. Normalizing the raw counts, detecting highly variable genes, finding clusters and creating t-distributed stochastic neighbour embedding (t-SNE) plots were done using the Seurat pipeline (version 3.2.3). Differential expression analysis for marker gene identification per subpopulation was based on the non-parametric Wilcoxon rank sum test implemented within the Seurat pipeline. Clusters with the same cell annotation based on gene expression analysis were combined to generate a more comprehensible dataset. Potential doublets were identified using the DoubletFinder algorithm (version 2.0.0)[51]. The number of high-confidence doublets was below 1% (113 out of 11,313 cells for the mock-treated sample and 96 out of 9,640 cells for the cytokinin-treated sample). Relative proportions of cell identities for both the mock- and cytokinin-treated samples were comparable (Supplementary Fig. 3d) to that of a previously published root meristem scRNA-seq atlas[18].

scRNA-seq: gene selection, cloning and plant transformation. Genes were selected on the basis of their cell type-specific differential expression between treatments. Transcriptional reporter lines were obtained by amplifying the upstream region of the transcriptional start and cloning this into the pGGA000 entry vector. The final expression clones were generated by cloning the promoter regions, three fluorescent tags (GFP), a HEAT SHOCK PROTEIN 18.2 (HSP18.2) terminator and a linker into the pFASTR-AG destination vector using Golden Gate cloning. All constructs were verified by Sanger sequencing and transformed into wild type using simplified floral dipping[52]. All primer sequences used for cloning and sequencing can be found in Supplementary Data 3.

Quantification and statistical analysis. All microscopic images were quantified using ImageJ and final figures were composed using Adobe Illustrator. For all expression pattern analyses, at least five independent transgenic lines showed the same expression pattern. For the expression pattern analysis and changes upon DEX treatments, at least three biological repeats with individual lines show similar results. For TCSn quantification, a rectangular area was selected from the quiescent center to the top of the image comprising the pericycle and all cells inwards. The pixel intensities from the entire selected area were analysed on root meristems of 7-day-old seedlings. Confocal images were all made through the quiescent center to ensure that the same position in the root was analysed in all images. Over 20 individual roots were imaged for each line. All statistical analysis plots were generated using the PlotsOfData webtool at standard settings (https://huygens.science.uva.nl/PlotsOfData/). In all boxplots, boxes represent the 1st and 3rd quartiles, and the centre line represents the median. The lowercase letters associated with the boxplots indicate significantly different groups as determined by one-way analysis of variance (ANOVA) with post-hoc Tukey HSD testing ($P < 0.001$).

Reporting Summary. Further information on research design is available in the Nature Research Reporting Summary linked to this article.

Data availability

Upon acceptance, the scRNA-seq data will be made accessible via an on-line browser tool (http://bioit3.irc.ugent.be/plant-sc-atlas/) and raw data can be accessed at NCBI with GEO number GSE179820. All other data are either in the main paper or the Supplementary Material. Source data are provided with this paper. Requests should be directed to the corresponding authors.

Received: 5 March 2021; Accepted: 6 October 2021;
Published online: 15 November 2021

References

1. Lucas, W. J. et al. The plant vascular system: evolution, development and functions. *J. Integr. Plant Biol.* **55**, 294–388 (2013).
2. De Rybel, B., Mähönen, A. P., Helariutta, Y. & Weijers, D. Plant vascular development: from early specification to differentiation. *Nat. Rev. Mol. Cell Biol.* **17**, 30–40 (2016).
3. Bishopp, A. et al. A mutually inhibitory interaction between auxin and cytokinin specifies vascular pattern in roots. *Curr. Biol.* **21**, 917–926 (2011).
4. De Rybel, B. et al. Plant development. Integration of growth and patterning during vascular tissue formation in *Arabidopsis*. *Science* **345**, 1255215 (2014).
5. Ohashi-Ito, K. et al. A bHLH complex activates vascular cell division via cytokinin action in root apical meristem. *Curr. Biol.* **24**, 2053–2058 (2014).
6. De Rybel, B. et al. A bHLH complex controls embryonic vascular tissue establishment and indeterminate growth in *Arabidopsis*. *Dev. Cell* **24**, 426–437 (2013).
7. Katayama, H. et al. A negative feedback loop controlling bHLH complexes is involved in vascular cell division and differentiation in the root apical meristem. *Curr. Biol.* **25**, 3144–3150 (2015).
8. Ohashi-Ito, K. & Bergmann, D. C. Regulation of the *Arabidopsis* root vascular initial population by LONESOME HIGHWAY. *Development* **134**, 2959–2968 (2007).
9. Ohashi-Ito, K., Matsukawa, M. & Fukuda, H. An atypical bHLH transcription factor regulates early xylem development downstream of auxin. *Plant Cell Physiol.* **54**, 398–405 (2013).
10. Ohashi-Ito, K., Oguchi, M., Kojima, M., Sakakibara, H. & Fukuda, H. Auxin-associated initiation of vascular cell differentiation by LONESOME HIGHWAY. *Development* **140**, 765–769 (2013).
11. Vera-Sirera, F. et al. A bHLH-based feedback loop restricts vascular cell proliferation in plants. *Dev. Cell* **35**, 432–443 (2015).
12. Miyashima, S. et al. Mobile PEAR transcription factors integrate positional cues to prime cambial growth. *Nature* **565**, 490–494 (2019).
13. Smet, W. et al. DOF2.1 controls cytokinin-dependent vascular cell proliferation downstream of TMO5/LHW. *Curr. Biol.* **29**, 520–529.e6 (2019).
14. Wybouw, B. & De Rybel, B. Cytokinin - a developing story. *Trends Plant Sci.* **24**, 177–185 (2019).
15. Kuroha, T. et al. Functional analyses of LONELY GUY cytokinin-activating enzymes reveal the importance of the direct activation pathway in *Arabidopsis*. *Plant Cell* **21**, 3152–3169 (2009).
16. Tokunaga, H. et al. *Arabidopsis* lonely guy (LOG) multiple mutants reveal a central role of the LOG-dependent pathway in cytokinin activation. *Plant J.* **69**, 355–365 (2012).
17. Mähönen, A. P. et al. A novel two-component hybrid molecule regulates vascular morphogenesis of the *Arabidopsis* root. *Genes Dev.* **14**, 2938–2943 (2000).
18. Wendrich, J. R. et al. Vascular transcription factors guide plant epidermal responses to limiting phosphate conditions. *Science* **370**, eaay4970 (2020).
19. Xu, Z. et al. Functional genomic analysis of *Arabidopsis thaliana* glycoside hydrolase family 1. *Plant Mol. Biol.* **55**, 343–367 (2004).
20. Leah, R., Kigel, J., Svendsen, I. & Mundy, J. Biochemical and molecular characterization of a barley seed beta-glucosidase. *J. Biol. Chem.* **270**, 15789–15797 (1995).
21. Dharmawardhana, D. P., Ellis, B. E. & Carlson, J. E. A beta-glucosidase from lodgepole pine xylem specific for the lignin precursor coniferin. *Plant Physiol.* **107**, 331–339 (1995).
22. Brzobohatý, B. et al. Release of active cytokinin by a beta-glucosidase localized to the maize root meristem. *Science* **262**, 1051–1054 (1993).
23. Weijers, D. et al. An *Arabidopsis* Minute-like phenotype caused by a semi-dominant mutation in a RIBOSOMAL PROTEIN S5 gene. *Development* **128**, 4289–4299 (2001).
24. Bartrina, I., Otto, E., Strnad, M., Werner, T. & Schmülling, T. Cytokinin regulates the activity of reproductive meristems, flower organ size, ovule formation, and thus seed yield in *Arabidopsis thaliana*. *Plant Cell* **23**, 69–80 (2011).
25. Zurcher, E. et al. A robust and sensitive synthetic sensor to monitor the transcriptional output of the cytokinin signaling network in planta. *Plant Physiol.* **161**, 1066–1075 (2013).
26. Werner, T., Motyka, V., Strnad, M. & Schmülling, T. Regulation of plant growth by cytokinin. *Proc. Natl Acad. Sci. USA* **98**, 10487–10492 (2001).

27. Matsumoto-Kitano, M. et al. Cytokinins are central regulators of cambial activity. *Proc. Natl Acad. Sci. USA* **105**, 20027–20031 (2008).
28. Schmülling, T. et al. Structure and function of cytokinin oxidase/dehydrogenase genes of maize, rice, *Arabidopsis* and other species. *J. Plant Res.* **116**, 241–252 (2003).
29. Lee, D. J. et al. Genome-wide expression profiling of ARABIDOPSIS RESPONSE REGULATOR 7(ARR7) overexpression in cytokinin response. *Mol. Genet. Genomics* **277**, 115–137 (2007).
30. Rashotte, A. M., Carson, S. D., To, J. P. & Kieber, J. J. Expression profiling of cytokinin action in *Arabidopsis*. *Plant Physiol.* **132**, 1998–2011 (2003).
31. Cui, H. et al. Genome-wide direct target analysis reveals a role for SHORT-ROOT in root vascular patterning through cytokinin homeostasis. *Plant Physiol.* **157**, 1221–1231 (2011).
32. Marquès-Bueno, M. D. M. et al. A versatile Multisite Gateway-compatible promoter and transgenic line collection for cell type-specific functional genomics in *Arabidopsis*. *Plant J.* **85**, 320–333 (2016).
33. Levesque, M. P. et al. Whole-genome analysis of the SHORT-ROOT developmental pathway in *Arabidopsis*. *PLoS Biol.* **4**, e143 (2006).
34. Mellor, N. et al. Theoretical approaches to understanding root vascular patterning: a consensus between recent models. *J. Exp. Bot.* **68**, 5–16 (2017).
35. Mähönen, A. P. et al. Cytokinin signaling and its inhibitor AHP6 regulate cell fate during vascular development. *Science* **311**, 94–98 (2006).
36. Help, H., Mahonen, A. P., Helariutta, Y. & Bishopp, A. Bisymmetry in the embryonic root is dependent on cotyledon number and position. *Plant Signal. Behav.* **6**, 1837–1840 (2011).
37. Helariutta, Y. et al. The SHORT-ROOT gene controls radial patterning of the *Arabidopsis* root through radial signaling. *Cell* **101**, 555–567 (2000).
38. Nakajima, K., Sena, G., Nawy, T. & Benfey, P. N. Intercellular movement of the putative transcription factor SHR in root patterning. *Nature* **413**, 307–311 (2001).
39. Sozzani, R. et al. Spatiotemporal regulation of cell-cycle genes by SHORTROOT links patterning and growth. *Nature* **466**, 128–132 (2010).
40. Möller, B. K. et al. Auxin response cell-autonomously controls ground tissue initiation in the early *Arabidopsis* embryo. *Proc. Natl Acad. Sci. USA* **114**, E2533–E2539 (2017).
41. Karimi, M., Depicker, A. & Hilson, P. Recombinational cloning with plant gateway vectors. *Plant Physiol.* **145**, 1144–1154 (2007).
42. Lei, Y. et al. CRISPR-P: a web tool for synthetic single-guide RNA design of CRISPR-system in plants. *Mol. Plant* **7**, 1494–1496 (2014).
43. De Rybel, B. et al. A novel Aux/IAA28 signaling cascade activates GATA23-dependent specification of lateral root founder cell identity. *Curr. Biol.* **20**, 1697–1706 (2010).
44. Ursache, R., Andersen, T. G., Marhavý, P. & Geldner, N. A protocol for combining fluorescent proteins with histological stains for diverse cell wall components. *Plant J.* **93**, 399–412 (2018).
45. Hellemans, J., Mortier, G., De Paepe, A., Speleman, F. & Vandesompele, J. qBase relative quantification framework and software for management and automated analysis of real-time quantitative PCR data. *Genome Biol.* **8**, R19 (2007).
46. Gong, X. et al. SEUSS integrates gibberellin signaling with transcriptional inputs from the SHR-SCR-SCL3 module to regulate middle cortex formation in the *Arabidopsis* root. *Plant Physiol.* **170**, 1675–1683 (2016).
47. Svačinová, J. et al. A new approach for cytokinin isolation from *Arabidopsis* tissues using miniaturized purification: pipette tip solid-phase extraction. *Plant Methods* **8**, 17 (2012).
48. Rappsilber, J., Ishihama, Y. & Mann, M. Stop and go extraction tips for matrix-assisted laser desorption/ionization, nanoelectrospray, and LC/MS sample pretreatment in proteomics. *Anal. Chem.* **75**, 663–670 (2003).
49. Novák, O., Hauserová, E., Amakorová, P., Dolezal, K. & Strnad, M. Cytokinin profiling in plant tissues using ultra-performance liquid chromatography–electrospray tandem mass spectrometry. *Phytochemistry* **69**, 2214–2224 (2008).
50. Lun, A. T., Bach, K. & Marioni, J. C. Pooling across cells to normalize single-cell RNA sequencing data with many zero counts. *Genome Biol.* **17**, 75 (2016).
51. McGinnis, C. S., Murrow, L. M. & Gartner, Z. J. DoubletFinder: doublet detection in single-cell RNA sequencing data using artificial nearest neighbors. *Cell Syst.* **8**, 329–337.e324 (2019).
52. Clough, S. J. & Bent, A. F. Floral dip: a simplified method for *Agrobacterium*-mediated transformation of *Arabidopsis thaliana*. *Plant J.* **16**, 735–743 (1998).

Acknowledgements

We thank D. Weijers for sharing unpublished materials, T. Schmülling for sharing *ckx3*, ckx5 and *ckx3 ckx5* seeds and K. Ljung for stimulating discussions. This work was funded by The Research Foundation – Flanders (FWO; Odysseus II G0D0515N to B.D.R. and post-doc fellowship 1215820N to B.Y.); the Netherlands Organization for Scientific Research (NWO; VIDI 864.13.00) to W.S., J.R.W. and B.D.R.; Ghent University (BOF20/GOA/012 to M.M. and B.D.R., and BOF18/PDO/151 to J.R.W.); the European Research Council (ERC Starting Grant TORPEDO; 714055) to B.Y. and B.D.R.; the China Scholarship Council (file number 202009350010) to Y.S.; the Ministry of Education, Youth and Sports of the Czech Republic (European Regional Development Fund-Project 'Plants as a tool for sustainable global development' No. CZ.02.1.01/0.0/0.0/16_019/0000827) to O.N.; and the Internal Grant Agency of Palacký University (IGA_PrF_2021_011) to O.N.

Author contributions

B.D.R. and B.Y. conceived the project and designed experiments; F.B., L.P., I.P., K.H. and O.N. performed enzymatic assays and cytokinin measurements; J.N. produced and purified BGLU44 protein with the help of J.H.; M.M., K.V., T.E. and Y.S. analysed single-cell data; E.F. and A.B. performed the mathematical modelling; B.Y., M.M., Y.S., W.S. and J.R.W performed all other experiments; B.D.R. supervised the project; B.Y. and B.D.R. wrote the paper with input from all authors.

Competing interests

The authors declare no competing interests.

Additional information

Extended data is available for this paper at https://doi.org/10.1038/s41477-021-01017-6.

Supplementary information The online version contains supplementary material available at https://doi.org/10.1038/s41477-021-01017-6.

Correspondence and requests for materials should be addressed to BaoJun Yang or Bert De Rybel.

Peer review information *Nature Plants* thanks Hitoshi Sakakibara, Enrico Scarpella and the other, anonymous, reviewer(s) for their contribution to the peer review of this work.

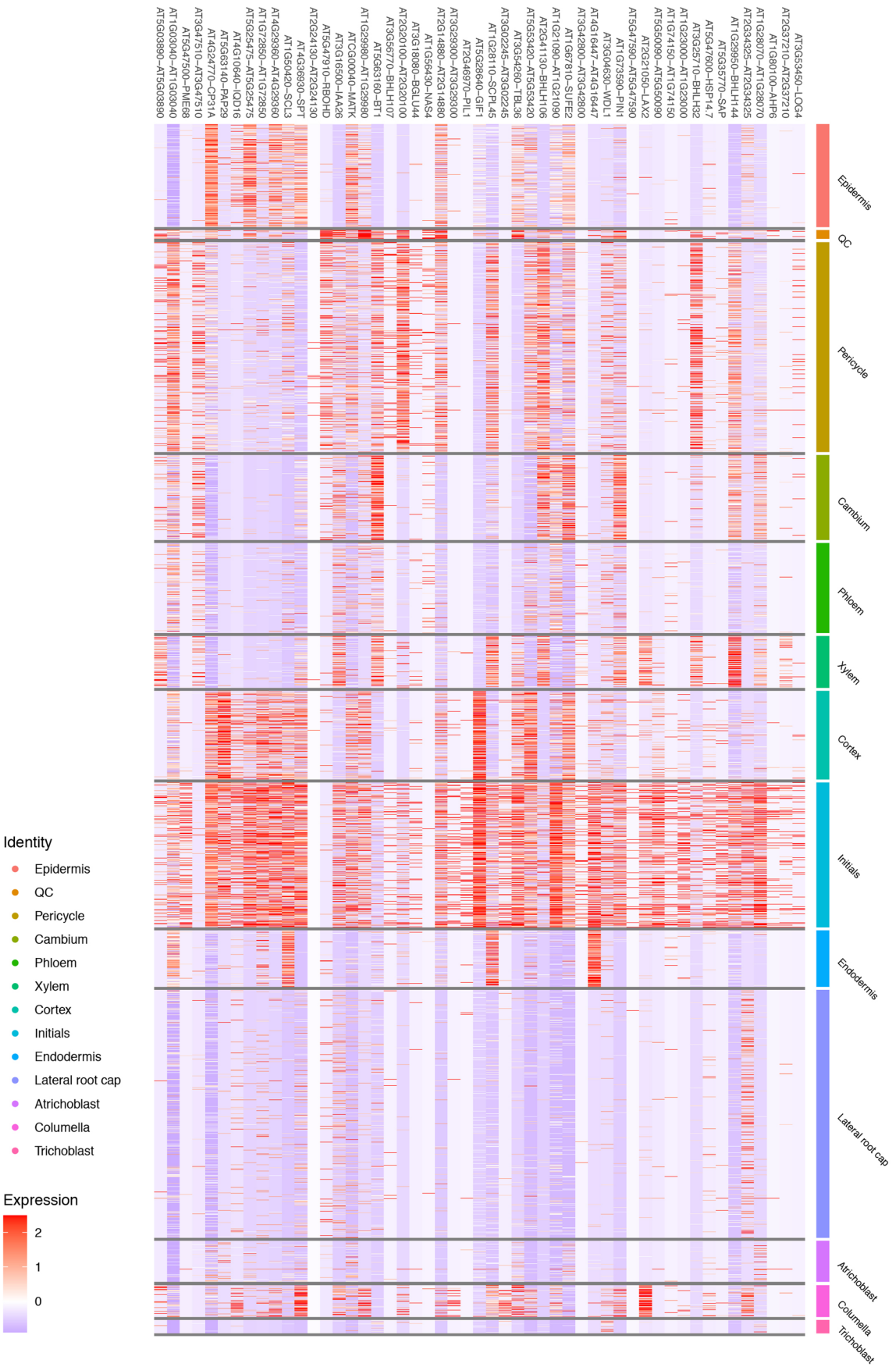

Extended Data Fig. 1 | *LOG4* single cell co-expression analysis. Top 50 genes co-expressed with *LOG4* according to a single cell atlas of the Arabidopsis root meristem. Expression values are shown for each of the separate tissue types.

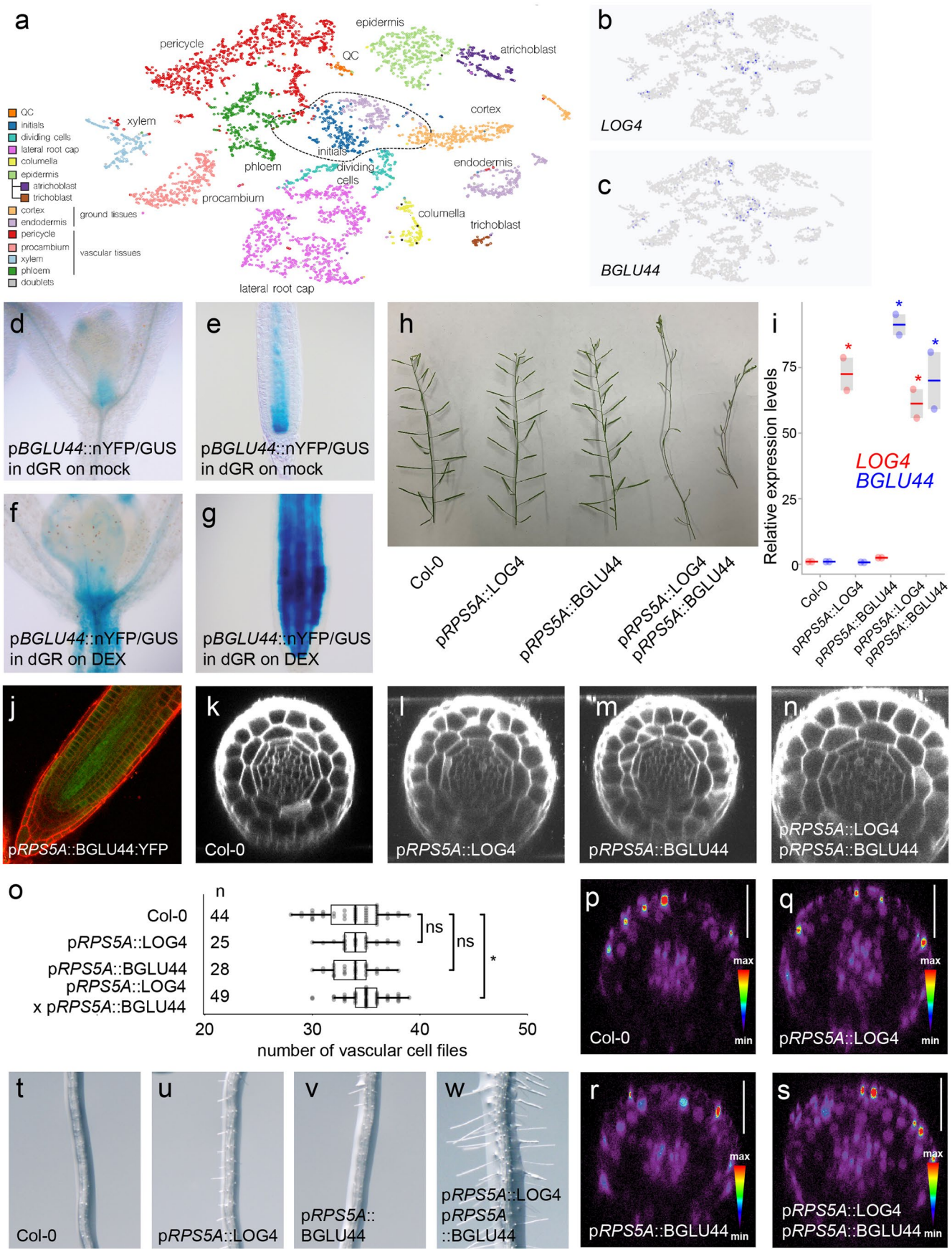

Extended Data Fig. 2 | See next page for caption.

Extended Data Fig. 2 | Characterization of *BGLU44* expression and function. a-c, Predicted expression of *LOG4* and *BGLU44* according to a single cell atlas of the Arabidopsis root meristem. Note the predicted co-expression in the feature plots for both genes. **d-g**, Expression of p*BGLU44*::nYFP/GUS in the dGR shoot and root meristems grown on mock medium and transferred to mock or 10 μM DEX for 24h. **h**, Inflorescence stem and silique phenotypes in the indicated genotypes. **i**, Relative expression levels as determined by RT-qPCR of *BGLU44* and *LOG4* in the indicated lines. Boxes represent the 1st and 3rd quartile and the center line represents the median. Asterisks in graphs indicate significance values as determined by standard two-sided t-tests. Black lines indicates mean values and grey boxes indicate data ranges. **j**, Expression of p*RPS5A*::BGLU44:YFP in the root meristem grown on mock medium showing that the BGLU44:YFP fusion protein is expressed. **k-o**, Phenotypes and quantification of the number of vascular cell files in the mentioned genotypes. Boxes represent the 1st and 3rd quartile and the center line represents the median. Statistics in n are performed using pairwise comparisons using a standard two sided t-test (p-value<0,05). **p-s**, Confocal images of optical cross sections of root meristems expressing pTCSn::ntdTomato reporter in the mentioned genotypes. Scale bars are 10 μm. **t-w**, Root hair phenotypes of the mentioned genotypes. In all panels, n represents the number of replicates or data points; all data and statistics are summarized in Supplementary Data 4. The experiments in j was repeated three times independently, with similar results.

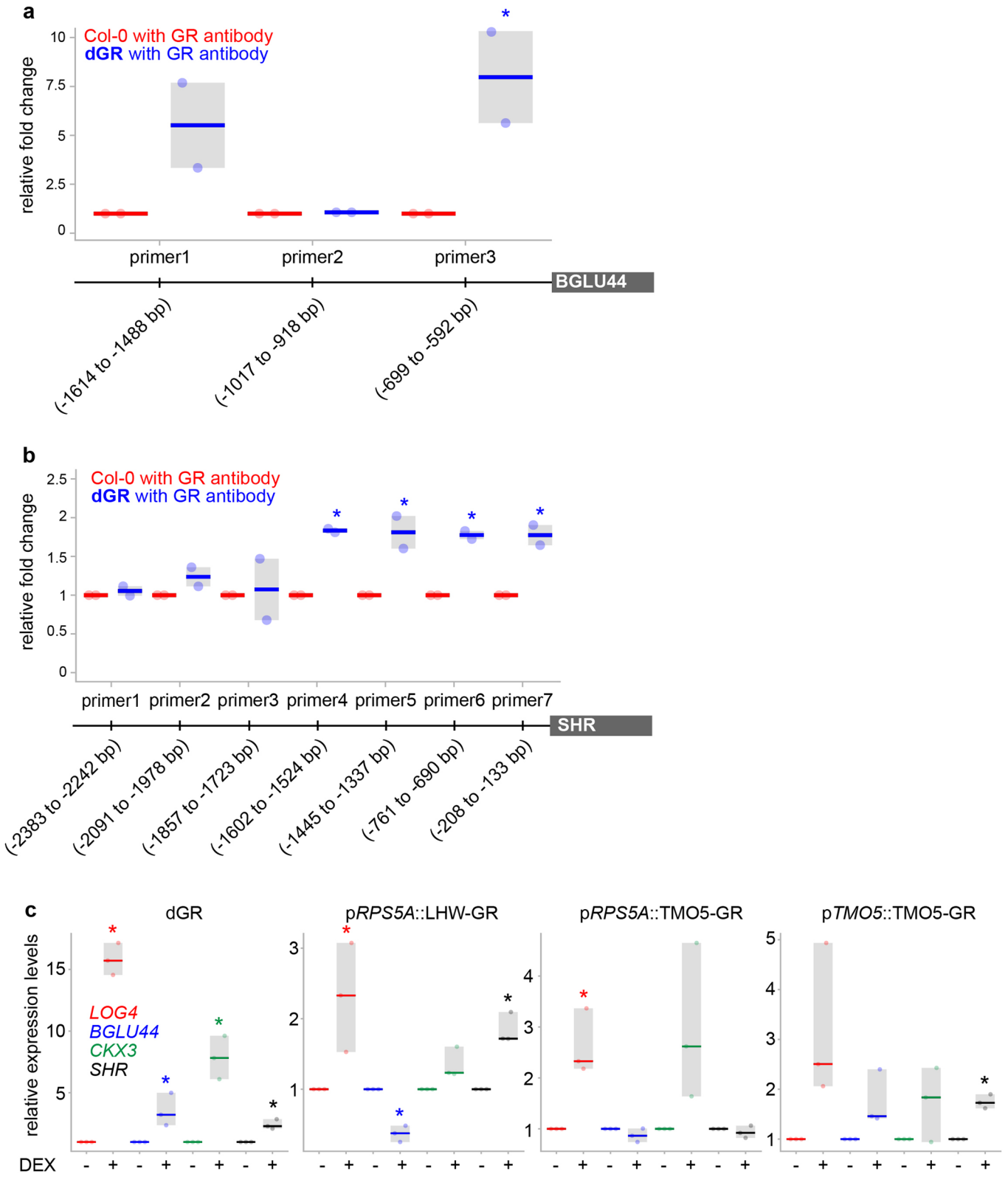

Extended Data Fig. 3 | *BGLU44* and *SHR* are direct TMO5/LHW target genes. a, **b**, ChIP-RT-qPCR experiments using anti-GR antibody on Col-0 and dGR lines. Graphs show the values of two biological repeats; black lines indicates mean values and grey boxes indicate data ranges. n = 2 biological replicates. Asterisks indicate significance values as determined by standard two-sided t-tests. **c**, Relative expression levels as determined by RT-qPCR of *LOG4*, *BGLU44*, *CKX3* and *SHR* in the indicated lines in presence or absence of 10μM DEX. n = 3 biological replicates. Asterisks in graphs indicate significance values as determined by standard two-sided t-tests. Black lines indicates mean values and grey boxes indicate data ranges. All Boxes represent the 1st and 3rd quartile and the center line represents the median. In all panels, n represents the.

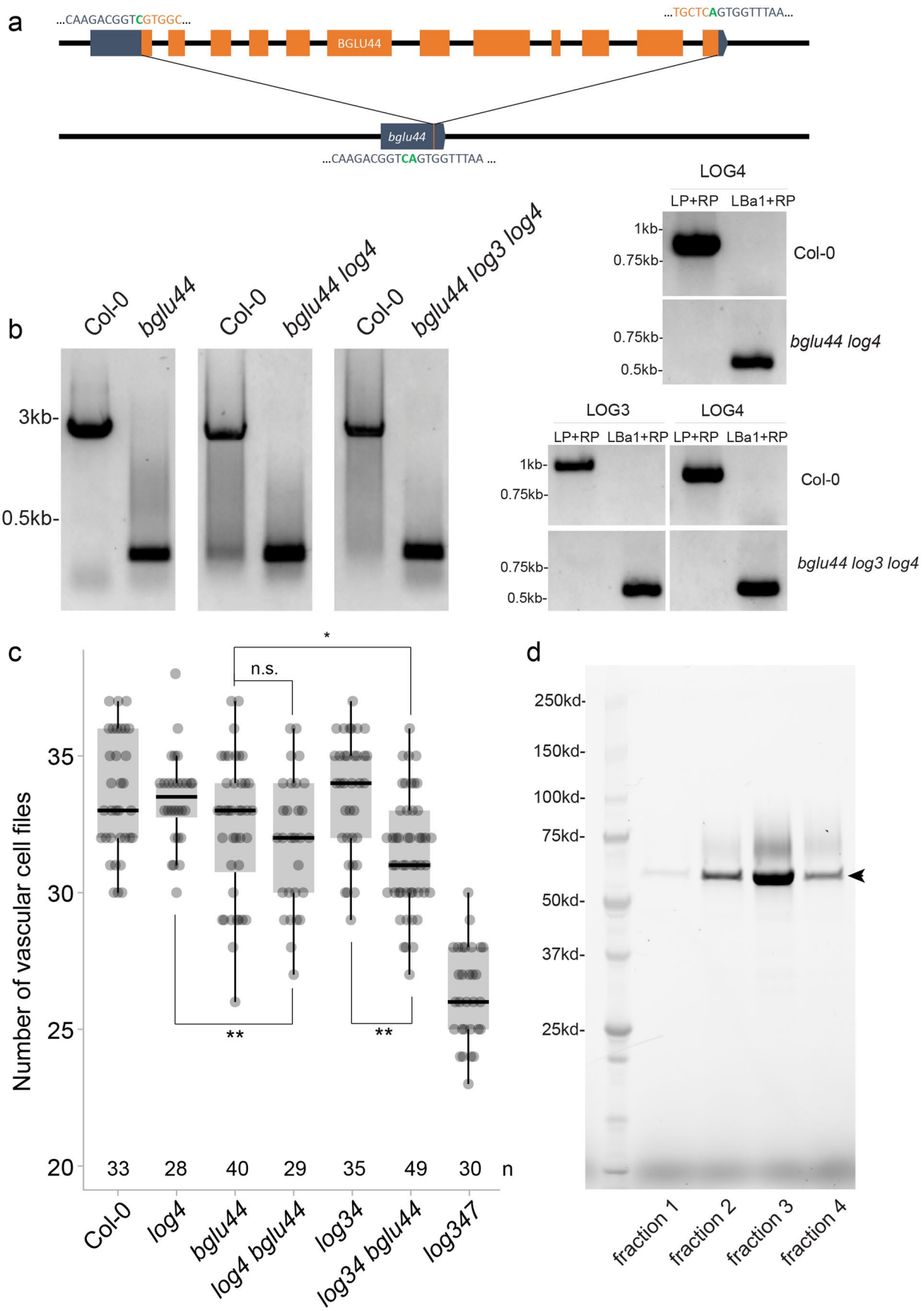

Extended Data Fig. 4 | See next page for caption.

Extended Data Fig. 4 | BGLU44 mutant generation and protein purification. a, Position of the deletion in the *bglu44* mutant line. **b**, PCR validation of the *bglu44* mutant and crosses with *log4* and *log34* mutants. **c**, quantification of the number of vascular cell files in the indicated lines. Boxes represent the 1st and 3rd quartile and the center line represents the median. n indicate independent plants, the data and statistics are summarized in Supplementary Data 4. Asterisks in graphs indicate significance values as determined by standard two-sided t-tests (*:p-value<0.05; **: p-value<0.01). **d**, Coomassie gel showing subsequent fractions of purified BGLU44 protein (arrowhead) after ion exchange chromatography. The experiments in b and d were repeated three times independently, with similar results.

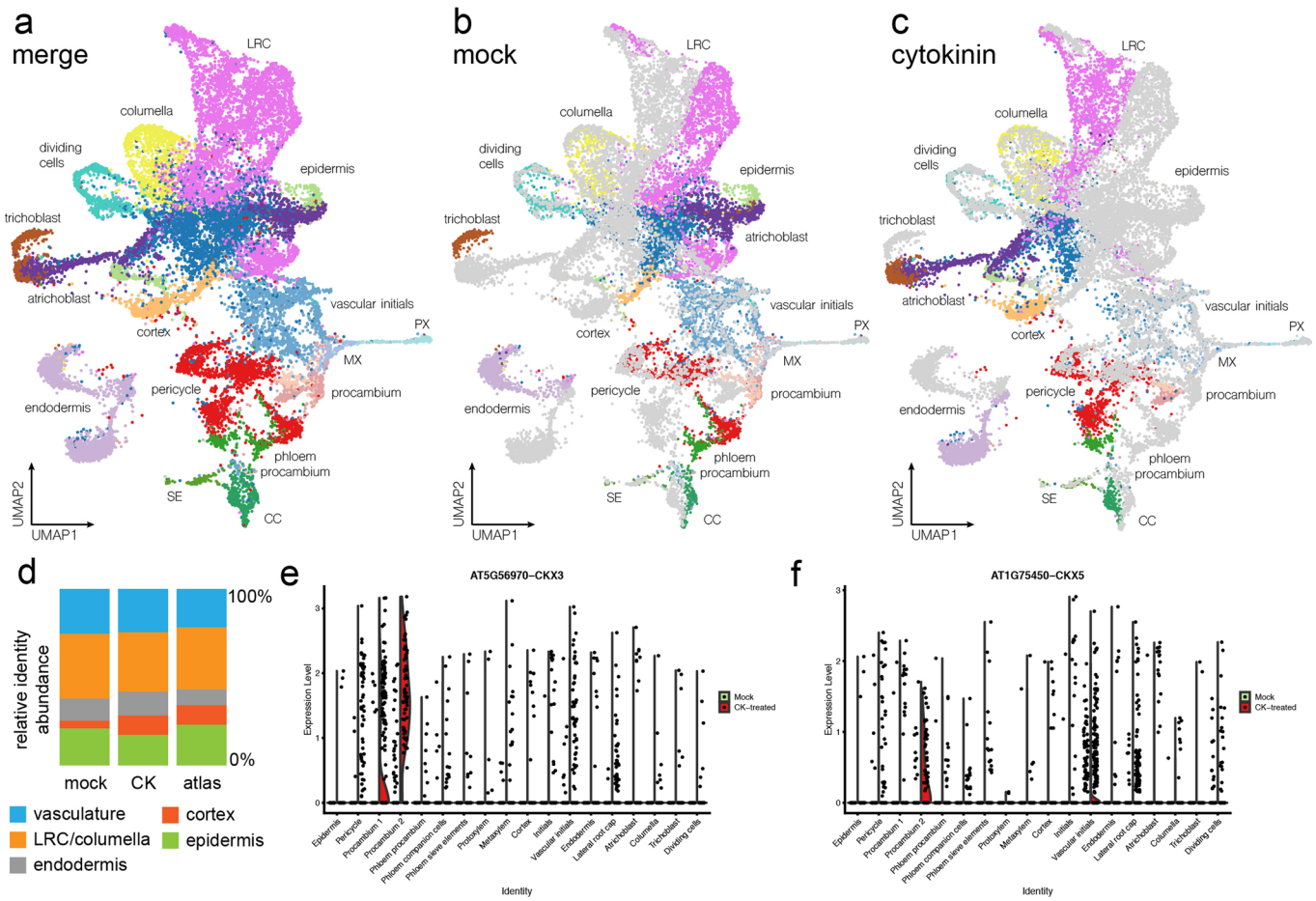

Extended Data Fig. 5 | Single cell transcriptional changes in root meristem cells upon cytokinin treatment. a-c. UMAP representation of the merged (a), mock (b) and cytokinin (c) datasets in which cell identities are shown by clusters of different colours. In panels b-c, the cells from the other dataset are indicated in grey to show contribution to each of the cell clusters. LRC: lateral root cap; PX: protoxylem; MX: metaxylem; SE: sieve element; CC: companion cell. The most central dark blue cell cluster is the initial cell cluster. **d**. Relative cell identity abundance in the mock and cytokinin (CK) datasets in comparison to a previously published root meristem atlas[8]. **e**,**f**. Violin plots showing normalized gene expression of *CKX3* (e) and *CKX5* (f) by cell type and split by treatment: left side of the violin is mock dataset in green; right side of the violin is CK-treated dataset in red).

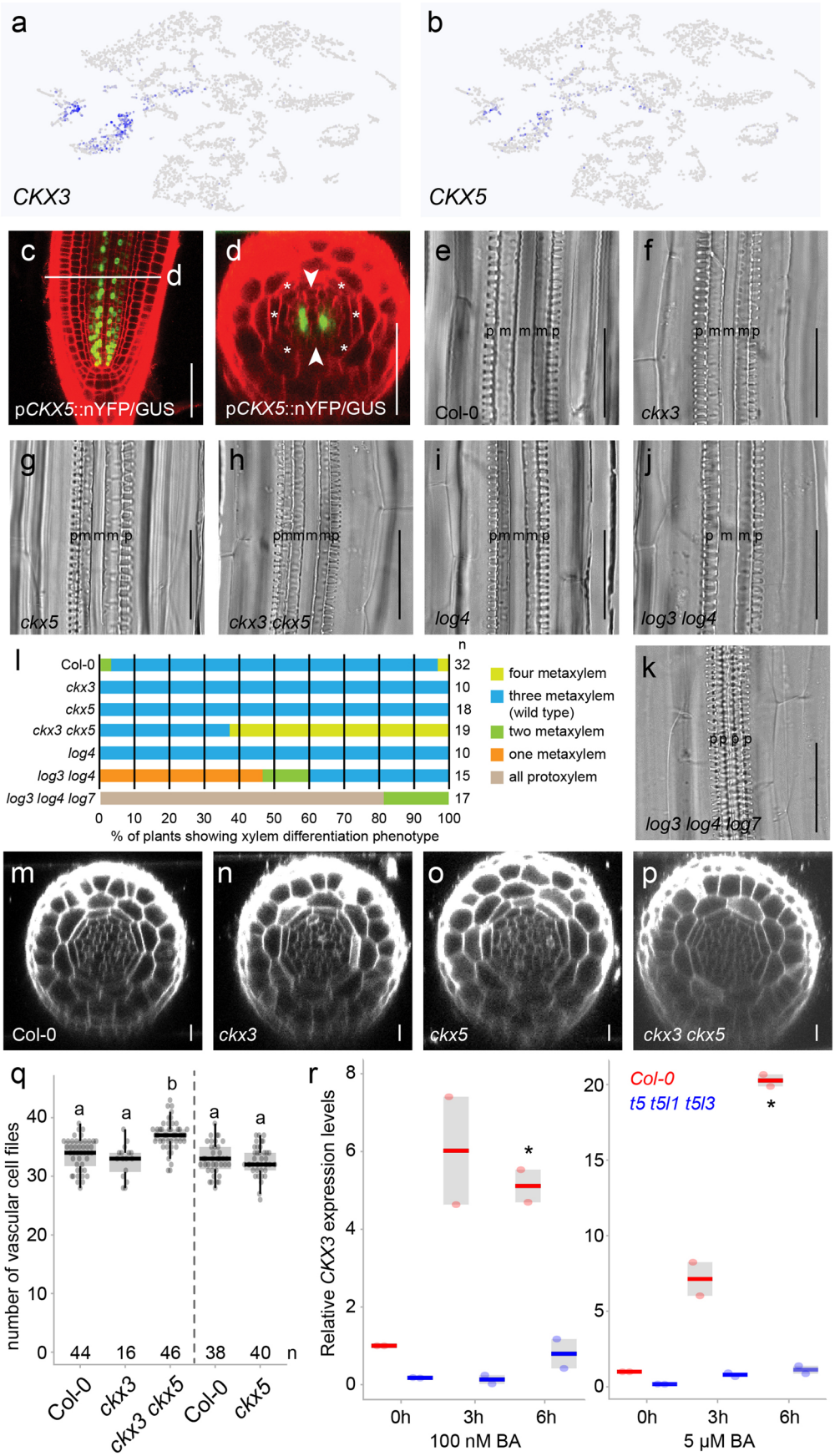

Extended Data Fig. 6 | See next page for caption.

Extended Data Fig. 6 | CKX3 and CKX5 are required for normal vascular development. a,**b**, Predicted expression of *CKX3* and *CKX5* according to a previously published single cell atlas of the Arabidopsis root meristem[18]. Compare to Supplementary Fig. 2a for cell identities. **c**,**d**, Expression of p*CKX5*::nYFP/GUS in the root meristem grown on mock medium. **e-k**, Microscopic images of xylem differentiation in the mentioned genotypes. p: protoxylem, m: metaxylem. **l**, Quantification of the different classes of xylem phenotypes shown in panels e-k. **m-p**, Confocal microscopy images of cross sections through the root meristem showing the vascular cell file number phenotype and quantification of the mentioned genotypes. **q**, Quantification of the number of vascular cell files shown in panels m-p. Lower-case letters on top of the boxplots indicate significantly different groups as determined by one-way ANOVA with post-hoc Tukey HSD testing ($p<0.001$). Boxes represent the 1st and 3rd quartile and the center line represents the median. Grey dotted line separates data from different experiments. **r**, RT-qPCR analysis showing the relative expression levels of *CKX3* on wild type Col-0 and *tmo5* triple mutant backgrounds when grown on mock (0h) or 100 nM or 5 μM BA for the indicated time. Boxes represent the 1st and 3rd quartile and the center line represents the median. n = 3 biological replicates. Asterisks in graphs indicate significance values as determined by standard two-sided t-tests. Black lines indicates mean values and grey boxes indicate data ranges. In all panels, n represents the number of replicates or data points; all data and statistics are summarized in Supplementary Data 4. The experiments in c-d were repeated three times independently, with similar results.

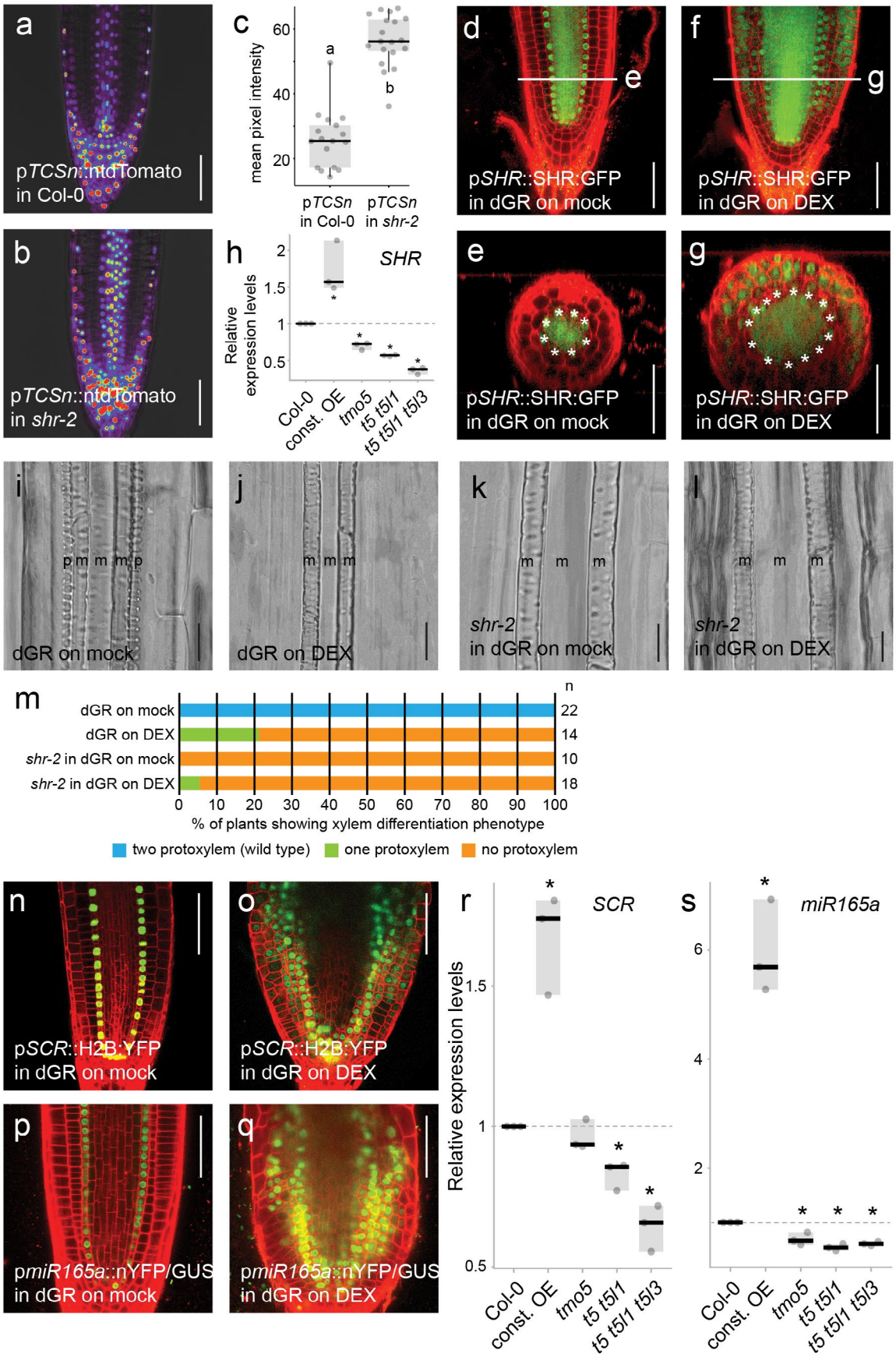

Extended Data Fig. 7 | See next page for caption.

Extended Data Fig. 7 | SHR acts downstream of TMO5/LHW. a,**b**, Confocal images of root meristems expressing pTCSn::ntdTomato reporter in Col-0 and *shr-2* backgrounds. **c**, Quantification of the pTCSn::ntdTomato mean pixel intensity in the mentioned genotypes. Boxes represent the 1st and 3rd quartile and the center line represents the median. n indicate independent plants. Lower-case letters on top of the boxplots indicate significantly different groups as determined by one-way ANOVA with post-hoc Tukey HSD testing ($p<0.001$). **d-g**, Expression of p*SHR*::SHR:GFP in the dGR root meristem grown on mock medium and transferred to mock or 10 μM DEX for 24 h. **h**, Relative expression levels of *SHR* in wild type (Col-0), TMO5/LHW misexpression, and *tmo5, tmo5 tmo5like1* (*t5 t5l1*) and *tmo5 tmo5like1 tmo5like3* (*t5 t5l1 t5l3*) mutant backgrounds. Asterisks indicate significance values as determined by standard two-sided t-tests. Boxes represent the 1st and 3rd quartile and the center line represents the median. n = 3 biological replicates. Black lines indicates mean values and grey boxes indicate data ranges. **i-l**, Microscopic images of xylem differentiation in the mentioned genotypes. p: protoxylem, m: metaxylem. **m**, Quantification of the different classes of xylem phenotypes shown in panels i-l. **n-o**, Expression of p*SCR*::H2B:nYFP in the dGR root meristem grown on mock medium and transferred to mock or 10 μM DEX for 24h. **p-q**, Expression of p*miR165a*::nYFP/GUS in the dGR root meristem grown on mock medium and transferred to mock or 10 μM DEX for 24h. **r-s**, Relative expression levels of *SCR* and *miR165a* in wild type (Col-0), TMO5/LHW misexpression, and *tmo5, tmo5 tmo5like1* (*t5 t5l1*) and *tmo5 tmo5like1 tmo5like3* (*t5 t5l1 t5l3*) mutant backgrounds. Boxes represent the 1st and 3rd quartile and the center line represents the median. n = 3 biological replicates. Asterisks indicate significance values as determined by standard two-sided t-tests. Black lines indicates mean values and grey boxes indicate data ranges. In panels a-b, d-g, i-l and n-q, scale bars are 50 μm. In all panels, n represents the number of replicates or data points; all data and statistics are summarized in Supplementary Data 4. The experiments in d-g, n-q were repeated three times independently, with similar results.

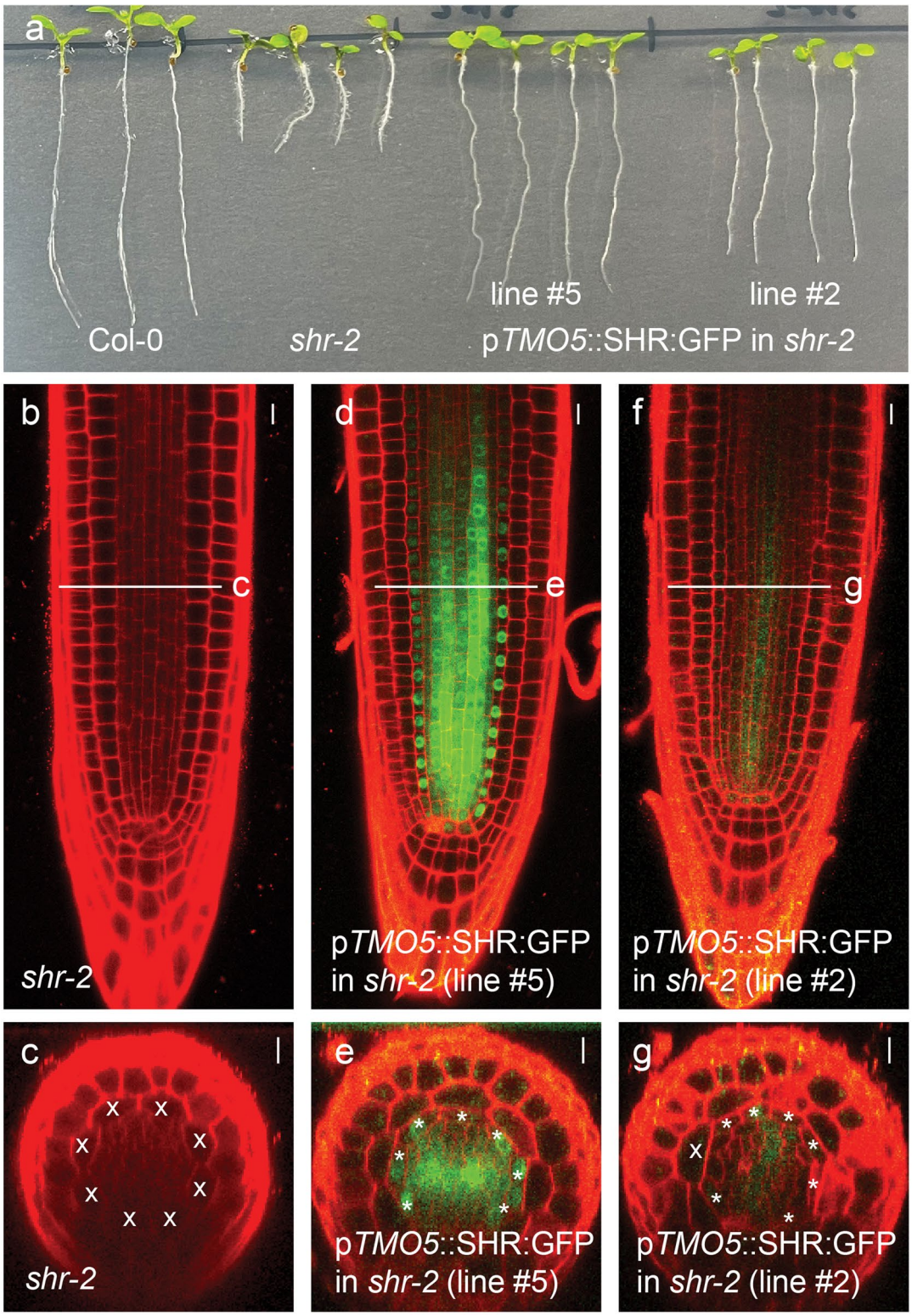

Extended Data Fig. 8 | Xylem expressed SHR is sufficient to rescue the *shr-2* mutant. a, Seedling phenotypes of the lines indicated. Note the rescue of root length in the p*TMO5*::SHR:GFP lines in shr-2 mutant background. **b-g**, Confocal images of root meristems of the indicated lines counterstained with PI (red). Scale bars are 10 µm. Panels c, e and g are optical cross sections of the images in b, d and f, respectively. Asterisks indicate endodermal cells; x marks mixed ground tissue identity. The experiments here were repeated three times independently, with similar results.

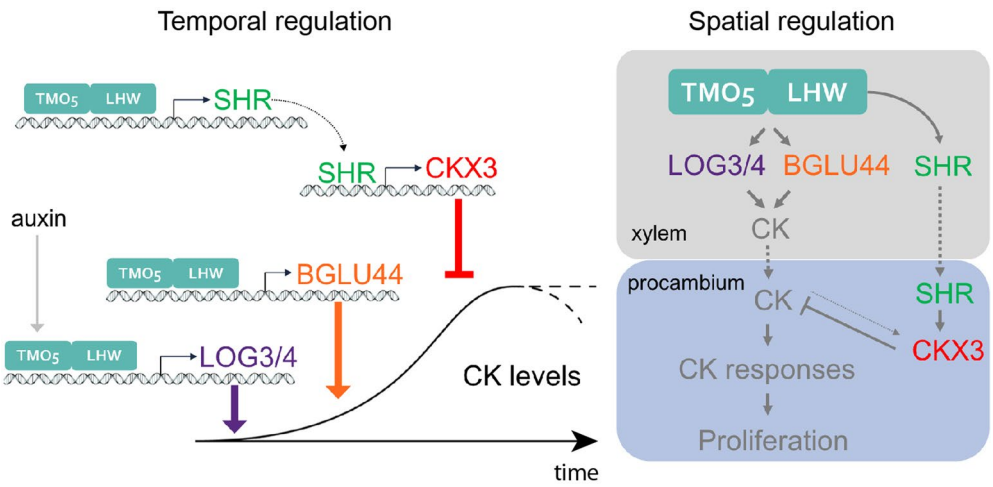

Extended Data Fig. 9 | A model for spatiotemporal control of cytokinin levels. Auxin induces *TMO5* expression and as such triggers activation of the TMO5/LHW heterodimer complex. Sequentially, *LOG3/4*, *BGLU44* and *SHR* expression are induced. SHR itself binds to the promoter region of *CKX3* to activate its expression. As such, the same transcription factor complex sequentially increases levels of active cytokinin via LOG3/4 and BGLU44; and represses levels active cytokinin via SHR-CKX3. The combined activity balances levels of active cytokinin to allow normal vascular proliferation and differentiation. The left side of the figures shows the temporal aspect, while the right side shows the spatial aspect.

nature research

Corresponding author(s): Bert De Rybel, Baojun Yang

Last updated by author(s): Sep 21, 2021

Reporting Summary

Nature Research wishes to improve the reproducibility of the work that we publish. This form provides structure for consistency and transparency in reporting. For further information on Nature Research policies, see our Editorial Policies and the Editorial Policy Checklist.

Statistics

For all statistical analyses, confirm that the following items are present in the figure legend, table legend, main text, or Methods section.

n/a	Confirmed
☐	☒ The exact sample size (*n*) for each experimental group/condition, given as a discrete number and unit of measurement
☐	☒ A statement on whether measurements were taken from distinct samples or whether the same sample was measured repeatedly
☐	☒ The statistical test(s) used AND whether they are one- or two-sided *Only common tests should be described solely by name; describe more complex techniques in the Methods section.*
☒	☐ A description of all covariates tested
☒	☐ A description of any assumptions or corrections, such as tests of normality and adjustment for multiple comparisons
☐	☒ A full description of the statistical parameters including central tendency (e.g. means) or other basic estimates (e.g. regression coefficient) AND variation (e.g. standard deviation) or associated estimates of uncertainty (e.g. confidence intervals)
☐	☒ For null hypothesis testing, the test statistic (e.g. *F*, *t*, *r*) with confidence intervals, effect sizes, degrees of freedom and *P* value noted *Give P values as exact values whenever suitable.*
☒	☐ For Bayesian analysis, information on the choice of priors and Markov chain Monte Carlo settings
☒	☐ For hierarchical and complex designs, identification of the appropriate level for tests and full reporting of outcomes
☒	☐ Estimates of effect sizes (e.g. Cohen's *d*, Pearson's *r*), indicating how they were calculated

Our web collection on statistics for biologists contains articles on many of the points above.

Software and code

Policy information about availability of computer code

Data collection	Olympus BX53 microscope, Leica SP8, LightCycler480 apparatus (Roche), NightSHADE LB 985 system (Berthold Technologies),Acquity UPLC® System (Waters, Milford, MA, USA)
Data analysis	Demultiplexing of the raw sequencing data was done by the 10x CellRanger (version 3.1.0) software 'cellranger mkfastq'. Reads were aligned to the Arabidopsis thaliana reference genome (Ensemble TAIR10.40) using 'cellranger count'. All analyses were performed in R (version 3.6.0). Pre-processing of the data was done by the scater (version 1.10.1) package according to the workflow proposed by the Marioni lab (Lun et al., 2016). Normalizing the raw counts, detecting highly variable genes, finding clusters and creating tSNE plots was done using the Seurat pipeline (version 3.2.3). Leica Application Suit X (version 3.3.0.16799) ImageJ (version,1.53c)

For manuscripts utilizing custom algorithms or software that are central to the research but not yet described in published literature, software must be made available to editors and reviewers. We strongly encourage code deposition in a community repository (e.g. GitHub). See the Nature Research guidelines for submitting code & software for further information.

Data

Policy information about availability of data

All manuscripts must include a data availability statement. This statement should provide the following information, where applicable:

- Accession codes, unique identifiers, or web links for publicly available datasets
- A list of figures that have associated raw data
- A description of any restrictions on data availability

All data generated or analyzed during this study were included in this published article and supplementary source data. Materials of this study are available from the corresponding author upon reasonable request. The single-cell data sets are available from indicated websites.

Field-specific reporting

Please select the one below that is the best fit for your research. If you are not sure, read the appropriate sections before making your selection.

☒ Life sciences ☐ Behavioural & social sciences ☐ Ecological, evolutionary & environmental sciences

For a reference copy of the document with all sections, see nature.com/documents/nr-reporting-summary-flat.pdf

Life sciences study design

All studies must disclose on these points even when the disclosure is negative.

Sample size	Sample sizes were determined by previous pilot experiments to be sufficient to achieve desired outcomes. Sample sizes are indicated in the Figures, legends and main text.
Data exclusions	No data was excluded in this study. In the single-cell analysis, outlier cells were excluded when they were 4 median absolute deviations (MADs) away from the median value of either library size or numer of expressed genes.
Replication	Each experiment was repeated at least twice, and only results representing the consistent outcome are reported.
Randomization	Plant samples used in this study were genetically homogeneous and of the same age with same growth condition. Plants were randomly picked from the larger pools for experiments.
Blinding	The experiments were carried out without prior knowledge of the experimental outcome. Therefore investigators were not blinded, but biological repeats were preformed as described above.

Reporting for specific materials, systems and methods

We require information from authors about some types of materials, experimental systems and methods used in many studies. Here, indicate whether each material, system or method listed is relevant to your study. If you are not sure if a list item applies to your research, read the appropriate section before selecting a response.

Materials & experimental systems

n/a	Involved in the study
☐	☒ Antibodies
☒	☐ Eukaryotic cell lines
☒	☐ Palaeontology and archaeology
☒	☐ Animals and other organisms
☒	☐ Human research participants
☒	☐ Clinical data
☒	☐ Dual use research of concern

Methods

n/a	Involved in the study
☒	☐ ChIP-seq
☒	☐ Flow cytometry
☒	☐ MRI-based neuroimaging

Antibodies

Antibodies used	Anti-GR antibody (polyclonal antibody, Catalog # PA1-516, LOT WB308073 Invitrogen)
Validation	This antibody had been successfully used in Arabidopsis for GR-fusion protein ChIP assay. (Morohashi et al, 2017. https://doi.org/10.1104/pp.107.104521)

Terms and Conditions

Springer Nature journal content, brought to you courtesy of Springer Nature Customer Service Center GmbH (“Springer Nature”).
Springer Nature supports a reasonable amount of sharing of research papers by authors, subscribers and authorised users (“Users”), for small-scale personal, non-commercial use provided that all copyright, trade and service marks and other proprietary notices are maintained. By accessing, sharing, receiving or otherwise using the Springer Nature journal content you agree to these terms of use (“Terms”). For these purposes, Springer Nature considers academic use (by researchers and students) to be non-commercial.
These Terms are supplementary and will apply in addition to any applicable website terms and conditions, a relevant site licence or a personal subscription. These Terms will prevail over any conflict or ambiguity with regards to the relevant terms, a site licence or a personal subscription (to the extent of the conflict or ambiguity only). For Creative Commons-licensed articles, the terms of the Creative Commons license used will apply.
We collect and use personal data to provide access to the Springer Nature journal content. We may also use these personal data internally within ResearchGate and Springer Nature and as agreed share it, in an anonymised way, for purposes of tracking, analysis and reporting. We will not otherwise disclose your personal data outside the ResearchGate or the Springer Nature group of companies unless we have your permission as detailed in the Privacy Policy.
While Users may use the Springer Nature journal content for small scale, personal non-commercial use, it is important to note that Users may not:

1. use such content for the purpose of providing other users with access on a regular or large scale basis or as a means to circumvent access control;
2. use such content where to do so would be considered a criminal or statutory offence in any jurisdiction, or gives rise to civil liability, or is otherwise unlawful;
3. falsely or misleadingly imply or suggest endorsement, approval , sponsorship, or association unless explicitly agreed to by Springer Nature in writing;
4. use bots or other automated methods to access the content or redirect messages
5. override any security feature or exclusionary protocol; or
6. share the content in order to create substitute for Springer Nature products or services or a systematic database of Springer Nature journal content.

In line with the restriction against commercial use, Springer Nature does not permit the creation of a product or service that creates revenue, royalties, rent or income from our content or its inclusion as part of a paid for service or for other commercial gain. Springer Nature journal content cannot be used for inter-library loans and librarians may not upload Springer Nature journal content on a large scale into their, or any other, institutional repository.
These terms of use are reviewed regularly and may be amended at any time. Springer Nature is not obligated to publish any information or content on this website and may remove it or features or functionality at our sole discretion, at any time with or without notice. Springer Nature may revoke this licence to you at any time and remove access to any copies of the Springer Nature journal content which have been saved.
To the fullest extent permitted by law, Springer Nature makes no warranties, representations or guarantees to Users, either express or implied with respect to the Springer nature journal content and all parties disclaim and waive any implied warranties or warranties imposed by law, including merchantability or fitness for any particular purpose.
Please note that these rights do not automatically extend to content, data or other material published by Springer Nature that may be licensed from third parties.
If you would like to use or distribute our Springer Nature journal content to a wider audience or on a regular basis or in any other manner not expressly permitted by these Terms, please contact Springer Nature at

onlineservice@springernature.com